THE GEOMETRY AND FLOW OF FIREWEED ROCK GLACIER, ALASKA

By

Adam Kyle Bucki

RECOMMENDED:

V. Romanovsky

W. D. Harrison

Keith Echelmeyer

Advisory Committee Chair

Paul W. Layer

Department Head

APPROVED:

Lawrence K. Duffy

Dean, College of Science, Engineering, and Mathematics

Dean of the Graduate School

4-16-02

Date

THE GEOMETRY AND FLOW OF FIREWEED ROCK GLACIER, ALASKA

A

THESIS

Presented to the Faculty

of the University of Alaska Fairbanks

in Partial Fulfillment of the Requirements

for the Degree of

MASTER OF SCIENCE

By

Adam Kyle Bucki, B.S.

Fairbanks, Alaska

May 2002

ABSTRACT

Little is known about the geometry, internal structure or flow of rock glaciers. Geophysical investigations were carried out on Fireweed Rock Glacier to define its geometry. Transient electromagnetic (TEM) methods were effective in determining its shape and depth as well as re-enforcing results of radar and seismic. All of these methods suggest a discontinuity at 15 to 30 m depth. The geometry acquired from these geophysical surveys was used to investigate the motion of the rock glacier. Analysis indicates that motion is concentrated in a pseudo-rectangular subsection of the larger valley on a "shear plane" at about 27 m depth. We infer that both deformation above and "sliding" along this shear plane contribute to the observed surface motion. This rock glacier flows relatively quickly for a rock glacier, and has seasonal and annual variations in speed. Some of the variations are related to the quasi-periodic calving at the terminus.

TABLE OF CONTENTS

LIST OF FIGURES

LIST OF TABLES

LIST OF APPENDICES

ACKNOWLEDGEMENTS

I extend many thanks to my parents for their continual understanding and support throughout all of my endeavors. My wife Carrie deserves equal credit for her patience and sacrifices — she has routinely picked up my slack in daily life. I am also in debt to Gretchen, Jonathan, Jennifer and Aidan who have given encouragement and support (even though Aidan doesn't know it yet). I apologize for completing a master's degree before either Jonathan and Gretchen and hope that doing so has provided them with some form of amusement or amazement. They were significantly more intent about school things than I was.

I give much credit to my advisor Keith Echelmeyer who has provided valuable suggestions and direction throughout my work. His interests expand well beyond glaciology and are an asset to any fieldwork, ski trip or canoe trip. I appreciate his time thinking about and discussing rock glaciers — even though they're quite slow. My project would not have been possible without Roger Elconin who got the ball rolling and provided a truly unique experience for myself and the rest of the glaciology lab at UAF. None of this work would have been possible without Roger's insight and motivation (even though he may not admit it). Will Harrison served on my advisory committee and offered many suggestions during the preparation of the manuscripts. Wills tenacity as a scientist and his good nature are an asset to the Glaciology Lab. Vladimir Romanovsky, a permafrost scientist, also served on my committee and brought diversity to our discussions of rock glaciers.

Fieldwork was made possible by the help of many individuals. Kevin Smith, Lilly Goodman, Dana Moudry, Patty Del Vecchio, Leif Cox and Martin Truffer all helped in the field. I hope that their experiences on Fireweed Rock Glacier were memorable and that their bodies have recovered fully from living on the rocks and hiking to Fireweed Mountain. I apologize to Leif for his first experience "hiking" out from the rock glacier — I needed the run. Also, Leif…don't forget your sleeping bag no matter how many H.A.B.F I prepare for you the night before a trip. Of all those that have visited, it was the K-9s that suffered the most. Tazlina, Cholly, Baxter and McKenzie gave up many paw pads during their visits.

Contributions to the geophysical work were made by Bob Hammond, Eugene Wescott and Zonge Engineering. I have also benefited from the suggestions and friendship of many others not yet mentioned: the rest of the Glaciers Lab — By Valentine, Sandy Zirnfeld, Anthony Arendt, Carl Benson, Craig Lingle, Dan Elsberg and Shad O'neel; my good friends —Ned Rozell, Kristen Bartecchi, Trilby Cox, Andy (no rear-view mirrors) Sterns and Andy (that crazy Brit) Mahoney. I would also like to extend my gratitude to the folks of McCarthy-Kennicott, Alaska.

I will always be grateful to my ski friends from Minnesota. Without their friendship it is unlikely I would have ever finished my B.S., let alone returned for my second year of college. I will always be grateful to Dave, Grant, Josie, Dan, Erik, Matt, Pete, Marcus, and Mark for the skiing and adventures. Many thanks go to E.O. Strack for showing me the secrets of ξ.

CHAPTER 1:

Introduction

Rock glaciers are poorly understood periglacial landforms that are mixtures of ice and rock that flow. They are typically associated with a talus slope that provides rock debris; however. the mechanism for ice accumulation is not understood. It is also unknown how the ice and rock debris interact to allow for motion. This lack of knowledge is in large part, due to the fact that information about the internal structure is difficult to acquire. Rock glaciers are covered by an unconsolidated layer of rock that is typically 2-3 m thick. This layer prevents direct observations of the internal structure. On Fireweed Rock Glacier (Fig. 1.1), a unique calving event provided a full transverse exposure of the internal structure, and was described by Elconin and LaChapelle (1997) and Elconin (1995).

Using the observations made by these authors, I employed a variety of geophysical methods that could be calibrated using the observed terminus exposure. With these methods, I was able to determine rock glacier geometry, which was then used to analyze rock glacier motion. For this analysis I also collected surface velocity data from a network of velocity markers. This network was initially established by Roger Elconin in 1994, and I have monitored it from 1999 to 2001.

Chapters 2 and 3 are manuscripts that will be submitted to the Journal of Glaciology. These papers are co-authored by my graduate advisor Keith Echelmeyer. Chapter 2 is a description of the methods and results of the geophysical work that I

conducted and emphasizes transient electromagnetic methods, which is seldom applied in glaciology. Chapter 3 is an analysis of the surface motion and terminus calving data, which utilizes the results presented in Chapter 2. Conclusions are given at the end of each chapter and then summarized in Chapter 4.

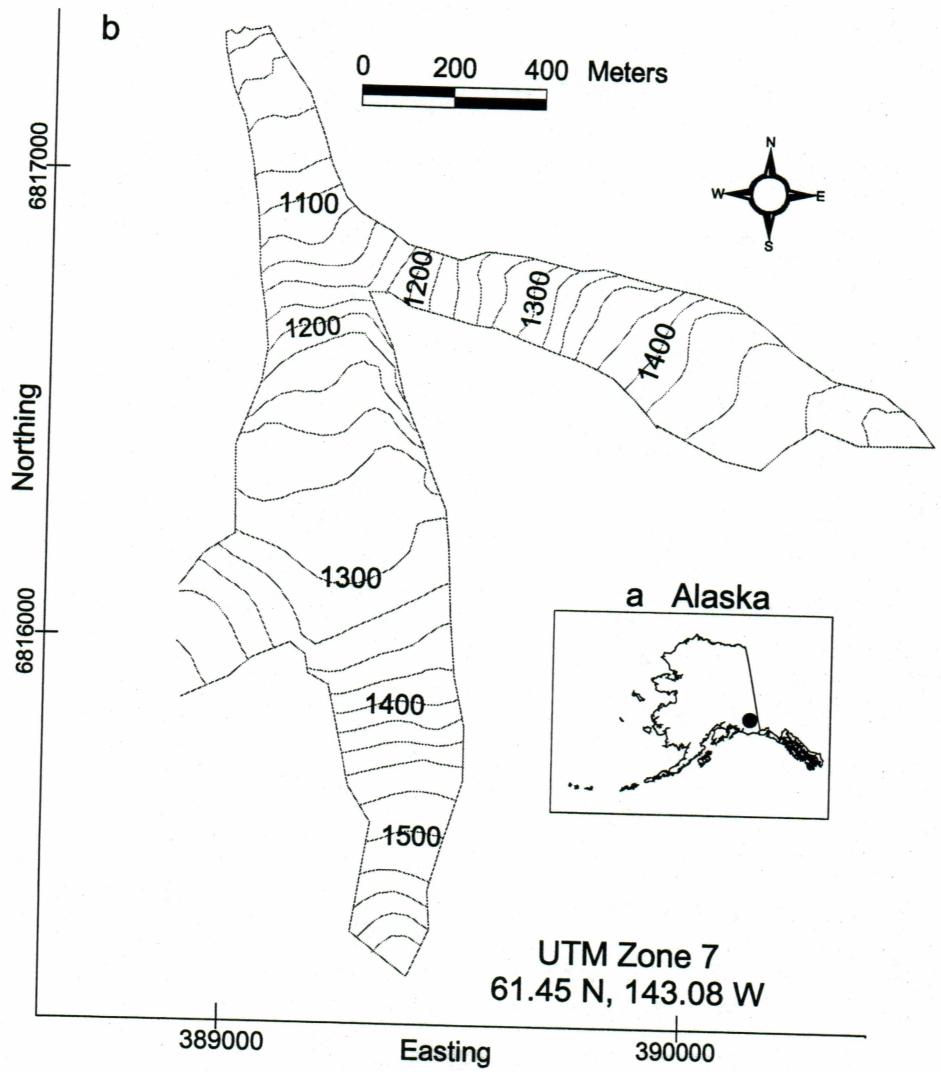

Fig 1.1: Location and map of Fireweed Rock Glacier.

CHAPTER 2:

Determination of Rock Glacier Thickness Using Transient Electromagnetic Methods[1]

ABSTRACT

Geophysical investigations on rock glaciers are often difficult because these glaciers are covered by an unconsolidated debris mantle a few meters thick, they are typically thin, and they are composed of an ice-rock mélange of unknown composition. Transient electromagnetic (TEM) methods allow some of these difficulties to be minimized, and data collection is relatively efficient. TEM, with calibration from terminus exposure, was used to determine the thickness (~ 60 m) of Fireweed Rock Glacier, Alaska under complex valley geometry. A conductive layer beneath the rock glacier was identified, and its distribution is consistent with a till-like layer. Corresponding results from seismic, radar and DC resistivity were limited. However, seismic refraction was used to resolve the debris mantle thickness (2 to 4 m), and it suggested the presence of a discontinuity at about 18 to 28 m depth within the mélange. The discontinuity was also weakly suggested by the ice radar and TEM data, and it has been found to be important in the flow of this rock glacier.

[1] This chapter will be submitted to the Journal of Glaciology as an instruments and methods paper.

INTRODUCTION

The thickness and cross-sectional shape of a rock glacier are important for understanding its stress distribution and motion. On ice glaciers this geometry is routinely determined using seismic and ice-radar methods. These methods are difficult to apply to rock glaciers because they are thinner, they are composed of a mixture of ice and rock of unknown composition, and they are covered by a layer of unconsolidated rock (the "debris mantle"). Radar is difficult because the absorption and scattering of radar waves are stronger in rock glacier mélange than in clean ice (Haeberli, 1985) and the basal interface may not be distinct. Seismic methods are complicated by the debris mantle, which limits the transfer energy from the source (usually an explosion) into the rock glacier and inhibits geophone coupling. Seismic field techniques have been devised to overcome these problems (Costello, 2000), but they are difficult to apply on a routine basis and have shown limited success. D.C. electrical resistivity has been widely used in rock glacier soundings (Fisch and others 1977; Evin and others, 1997), but the debris mantle again poses problems with electrical coupling and requires labor-intensive field setups. We have used all of these methods to investigate the geometry of Fireweed Rock Glacier with limited success. We have found that transient electromagnetic (TEM) methods provide the best means of investigating the thickness distribution. They do not require a high degree of physical or electrical coupling. Here we discuss our methods and the results for each of these techniques applied to Fireweed Rock Glacier.

DESCRIPTION OF THE ROCK GLACIER AND ITS GEOLOGIC SETTING

Fireweed Rock Glacier is 2 km long and flows down a steep, narrow valley on Fireweed Mountain, which is located in the Wrangell Mountains of southcentral Alaska (61.45 N, 143.08 W, see Fig. 2.1 Chapter 3). This is an active rock glacier that emanates from three separate cirques as independent tributaries, each having average surface slopes of about 15°. These tributaries coalesce to form the Main Trunk, which flows for about 500 m before it terminates at a 90 m-wide, quasi-periodically calving snout (Elconin and LaChapelle, 1997). Surface velocities on the Main Trunk are up to 3.5 m a^{-1}; these are relatively large compared to other rock glaciers (<1 m a^{-1}; Chapter 3). Within the Main Trunk, each tributary remains lithologically distinct, forming the East, Middle and West Flows. There are V-shaped longitudinal troughs between the flows that create an irregular transverse topographic profile. The longitudinal profile of the Main Trunk is much smoother and has an average slope of 11°.

The rock glacier occupies a cirque and valley complex that has likely contained a small ice glacier in the past, as indicated by the overall U-shaped valley. However, the lower portion of the Main Trunk fills a narrower V-shaped section that has been eroded into the bottom of the larger U-shaped valley. The Main Trunk narrows from 240 m in the upper portion to 90 m at the terminus, and the walls of the valley immediately above the rock glacier surface have slopes from 25° to 45°. Extrapolation of these slopes beneath the rock glacier suggests that the Main Trunk valley is at least 40 to 50 m deep along the centerline. The terminus face has a slope of 38° and has a centerline thickness

of 58 m (Chapter 3). This face is about 90 m wide at the top and narrows to about 10 to 15 m at the base, where a proglacial stream emanates.

Fireweed Mountain is a shallow pluton of Tertiary age that has invaded Cretaceous sediments with fine to medium grain felsic porphyry dikes and sills. Some of these intrusives are hydrothermally altered, with fine-grained pyrite crystals and centimeter-size feldspar crystals. The sedimentary rocks are mostly mudstones with a few thin beds of limestone; some of these are also hydrothermally altered. The Main Trunk of the rock glacier flows along a contact between altered and non-altered mudstone (MacKevett and Smith, 1972). The bedrock adjacent to the Main Trunk does not contribute material to the rock glacier surface; instead the debris is derived from talus cones in the cirques and along the upper portions of the tributaries (Elconin and LaChapelle, 1997).

GEOPHYSICAL METHODS AND RESULTS

Seismic Surveys

We attempted seismic reflection and refraction soundings using a 12-channel digital seismograph and a geophone spacing of 7 to 15 m. For sources we used 300 to 500-grain blank shotgun shells discharged within the debris mantle just below the surface. Geophones were placed in small pits and sandwiched between flat rocks in an attempt to reduce noise. Shot were made at various positions along and off the ends of transverse and longitudinal arrays.

No reflections were identified, probably because of poor source coupling and a low signal-to-noise ratio. We suspect that larger explosive sources may have penetrated the debris mantle more effectively. However, refraction analysis indicated a consistent pattern of first-arrivals and suggested the presence of three layers. Three longitudinal arrays on the Main Trunk and one on the Middle Tributary indicated a debris mantle seismic velocity of 400 to 500 m s^{-1}, with the second and third layers having velocities of about 1700-2300 m s^{-1} and about 4500 m s^{-1}, respectively (Fig. 2.2). We estimate a debris mantle thickness of 2 to 4 m, which is similar to that observed by Elconin and LaChapelle (1997) in moulins and crevasses. The thickness of the second layer is estimated to be 18 to 28 m. Extrapolations of valley wall geometry suggest that the base of this second layer thickness does not represent the valley bottom nor the valley walls, and we suspect that there may be a discontinuity within the rock glacier mélange at a depth of 20-27 m below the surface. This is further discussed in Chapter 3. However, the difficulty experienced with source/geophone coupling at the debris mantle precludes further detailed resolution of subsurface structure, including the base of the bottom layer.

Radio-echo Sounding

Thirty ice radar soundings were made with a ~5 MHz mono-pulse system. The antennas were orientated perpendicular to flow with a spacing of 30 to 50 m. The observed waveforms showed a distorted signal that may have been caused by the overlap of the airwave and a return wave, as is observed when sounding a very shallow glacier. Because of this interference, it was difficult to determine the timing of the return signal.

But in some cases we were able to estimate the travel time of the first return, typically in the range 0.12 μs to 0.19 μs. Using an electromagnetic wave velocity of 170 m μs^{-1} (clean ice) we obtained a reflector "depth" of 10 to 20 m. These possible returns were randomly distributed and exhibited no obvious spatial relationship, hence they were not used to define rock glacier geometry.

Electrical Resistivity

The electrical resistivity of the subsurface is a diagnostic physical property that can be determined with a variety of methods. Most often used in rock glacier surveys are DC resistivity methods (Vonder Mühll, 2001), in which the resistivity structure is determined by applying a voltage between electrodes placed in the substrate. Alternatively, induction methods determine resistivity by measuring an induced electromagnetic field. These induction methods are not often used in glaciology.

Laboratory Testing

To aid in our interpretation of electrical resistivity soundings, we tested the rock samples from the debris mantle and others inferred to underlie the Main Trunk. Our sampling indicates that the debris mantle on the West Flow contains 80% intrusive rock, a large portion of which is thermally altered. The mantle of the Middle Flow contains equal amounts of intrusive rocks and mudstone, and that on the East Flow has two compositionally distinct sections, the easternmost part having less thermally altered rock. We note that these compositions may not represent the relative concentrations of these

rock types at depth within the ice-rock mélange. Electrical resistivities of the samples were measured in the laboratory by Zonge Engineering using conventional time domain methods (Table 1). The altered intrusive rocks had quite low resistivities (~800 Ω m), while the non-altered igneous rocks and both mudstones had higher resistivities (>2000 Ω m). These measured resistivities are likely to be somewhat different than *in situ* values because of fractures and interstitial fluids, so we use them only as guidelines when interpreting our geophysical data. We also determined the resistivity of the proglacial stream water. It was quite high (~8500 Ω m), which indicates that it does not contain significant dissolved ions.

Transient Electromagnetic (TEM) Methods: Basic Principles

On Fireweed Rock Glacier we attempted DC resistivity measurements with dipole-dipole arrays. This array provides better lateral resolution than other standard array types (e.g. Schlumberger and Wenner arrays). However, relative to these other arrays, the dipole-dipole array is more sensitive to high electrode contact resistance (Hauck, 2001). In spite of considerable effort to overcome this limitation using, for example, brine soaked sponges at the electrodes, we did not acquire any interpretable data.

We then attempted the transient electromagnetic (TEM) methods. These do not require direct electrical coupling with the debris mantle. The system configuration used in this study is shown in Figure 2.3, and is referred to as an "in-loop" array. With TEM,

the resistivity of the subsurface is determined by measuring the diffusive decay of induced currents. These currents are generated by applying a current in the large outer transmitting loop to create a primary magnetic field. Abruptly shutting this current off causes eddy currents to be induced in the substrate according to Faraday's Law. These new currents generate their own secondary magnetic fields that decay with a rate proportional to the electrical resistivity of the subsurface. This decaying magnetic field is measured with the smaller receiver loop shown in Figure 2.3. This coplanar loop geometry is used to measure the vertical component of the transient field, H_z.

It has been shown by Nabighian (1979) that the combined effect of all induced currents in a uniform half-space can be approximated by a single current "loop" moving downward with a velocity v given by

$$v = \left(\frac{4\rho}{\pi\mu t} \right)^{1/2} \qquad (1)$$

where ρ is the resistivity of the half-space, μ is its magnetic permeability and t is the time since the turnoff of the primary magnetic field. This current loop expands like a "smoke ring" from the center of the loop on the surface at an angle of 35 to 45°. In a layered half-space the current filament moves with varying velocity as it crosses layer boundaries. If it encounters a layer with a very low resistivity, its velocity is reduced, and it can be trapped inside such a layer (Nabighian and Macnae, 1987). A TEM sounding is a measurement, normally made at the surface, of the time rate of change of the magnetic field generated by this propagating current loop.

For in-loop soundings it is useful to consider the analytic solution for the response at the surface of a uniform half-space of resistivity ρ given by Kaufman (1979). He determined that for a circular in-loop geometry with transmitter radius a and current I, the decay of the vertical component of the magnetic field at the surface takes the form

$$\frac{\partial H_z}{\partial t} = -\frac{I\rho}{\mu_0 a^3}\left[3erf(\theta a) - \frac{2}{\pi^{1/2}}\theta a(3+2\theta^2 a^2)e^{-\theta^2 a^2}\right] \quad (2)$$

where

$$\theta = \left(\frac{\mu_0}{4t\rho}\right)^{1/2} \quad (3)$$

μ_0 is the permeability of free space and t is the time after immediate turn off of the primary magnetic field. This theoretical transient response is shown in Figure 2.4a for a transmitter with radius 11 m and a current of 3.5 A. The response can be divided into three stages: early-time, intermediate-time and late-time. The time at which these stages occur is determined by the product θa in Equations (2) and (3). In the early-time ($\theta a >> 1$) the second term of Equation (2) is small and the rate of change of the magnetic field is nearly constant, with a value that is proportional to the resistivity of the half-space (early-time segment in Fig. 2.4). Intermediate-time is the transition from the early-time response to the late-time response. For a given transmitter geometry (constant a) the resistivity of the half-space influences how quickly this transition is made. This is illustrated in Figure 2.4a, where the responses of two half-spaces having 90 Ω m and 20 Ω m resistivities are compared. At late-time, the product θa is small, and Equation (2) can be approximated by

$$\frac{dH_z}{dt} \approx \frac{I\mu_0^{3/2} a^2}{20\pi^{1/2}\rho^{3/2}} t^{-k} \qquad (4)$$

where $k = 2.5$ for a uniform half-space, as shown in Figure 2.4. Over layered geology it is observed that k can vary from about 1.5 to 3.5. These changes in the slope of the decay curve can be used to infer the presence of layers of different resistivities. It follows from this simplified model that the response at a given time is an indicator of the resistivity at a given depth. However, this relationship is not necessarily one to one.

In reality, at some point in time the induced currents decay to levels such that their signal becomes noisy relative to background or ambient electromagnetic levels. This causes the decay curves in Figure 2.4a to show increased scatter and a leveling out in time. However, this is not observed if there exists a significantly shallow, low resistivity object (3-D "conductor"), such as a slab or sphere. Conductors exhibit an exponentially decaying field rather than the power-law decay of the half-space (Eqn. 4), as given by

$$\frac{\partial H}{\partial t} \approx A_0 e^{-t/\tau} \qquad (5)$$

where A_0 encompasses geometric parameters and τ is the characteristic time of the conductor. The characteristic time contains information on the dimensions and resistivity of the object (Nabighian and Macnae, 1991). When a conductor is situated within a half-space, the decay curve has contributions from both the half-space and the conductor. Because of the difference in decay between a half-space (typically resistive) and a conductor, a conductor's decay can be recognized, if its characteristic time is large enough, because its signal persists after the half-space response has decayed to

background levels. As a simplification, Equations (2) and (5) can be superimposed, as shown in Figure 2.4b for various values of τ and $A_0 = 30$. Here, we distinguish between two stages: late-time I and a late-time II. In late-time I the decay follows a power-law (Eqn. 4). In late-time II the decay either becomes noisy as a result of background electromagnetic levels or, if a conductor is present, the decay is much less noisy and follows the exponential in Equation (5).

Transient decay curves contain a significant amount of detail about the subsurface resistivity structure; however, this structure is not directly apparent in the decay curves themselves. To more clearly express the resistivity structure of the subsurface, the decay curves need to be re-parameterized into resistivity-depth curves through inversion. This is often done by converting a decay curve into either apparent resistivity or a curve of "smooth-model" resistivity. Apparent resistivity curves are determined by the departures of a decay curve from a uniform half-space response (Kaufman and Keller, 1983). Smooth-model inversion assumes a multi-layered resistivity structure and solves for a distribution of resistivity in these layers that is sufficiently smooth (Ward and Hohmann, 1987). This later approach can provide more detail about the subsurface than apparent resistivity calculations because it incorporates the time rate of change of the magnetic field, not just the measured magnitude of the magnetic field at a point in time. Smooth-model resistivities are also a complete solution to the layered-earth response, and they provide realistic values of the true resistivity as opposed to the averaging effects of apparent resistivity. Both are one dimensional, with assumed planar geometry. The

smooth-modeling software used in this study was developed by Zonge Engineering (Tucson, Arizona).

If a series of soundings is made along a transect (in our case, either longitudinal or transverse on the rock glacier surface), then the resulting series of smooth-model inversions can be plotted in a pseudo-section showing contours of resistivity at depth along a transect.

Summarizing the expected structure of the TEM decay curves, we note there are several key features. The nearly constant level of the early phase and its duration give some information about the overall resistivity of the upper layers. Change in the slope of the late-time I stage represents resistivity changes with depth, whereas the late-time II stage can indicate the presence and "strength" of buried conductors.

Errors in TEM Measurements

Geometric errors in TEM measurements occur if there are deviations from the assumed shape and relationship of the transmitter and receiver loops. For this reason, it is important to maintain consistent loop geometries throughout a survey. However, this is less critical than in frequency-domain measurements, because in TEM the induced field is measured when the transmitter is off. Topographic effects can also introduce error in TEM soundings but, unlike D.C. resistivity methods, these are often reduced by simply accounting for the relative positions of different soundings. Cultural features such as power lines, large metallic objects, and VLF radio signals can negatively affect TEM.

Consideration of induced polarization (IP) is also required. IP effects can "mask" the transient response in a TEM measurement. We note that ice does exhibit polarization within the frequencies typical of TEM systems; however, the displacement currents from the induced polarization are likely to be small relative to the induced currents (Keller, 1991; Petrenko and Whitworth, 1999).

TEM Instrumentation

The effective depth of investigation for TEM sounding depends on the size of the transmitter loop, background noise and resistivity of the substrate. The rate at which the current can be shut off in the transmitter loop prior to measurements is a limiting factor in resolving shallow depths. Rock glaciers can be considered shallow, so rapid termination of the transmitter current is required. Systems that employ such a rapid turn-off (~1.5 μs) are capable of depth resolution of a few meters, even in resistive substrates.

We used the NanoTEM® system developed by Zonge Engineering for our survey (Fig. 2.3). This system collects a series of data at 31 progressive time windows per measurement, and 400-1000 individual measurements (made at 32 Hz) are stacked to compose a sounding. For each measurement, data collection begins at about 1.5 μs and extends to 3 ms after transmitter turn-off. These data define the decay of the magnetic field in a curve similar to those shown in Figure 2.5. For smooth-model inversions the earliest time window is often discarded because it is sensitive to the transmitter turn-off. The noisy results late in the record (at the end of late-time II) are also discarded.

NanoTEM Data

Ten in-loop soundings were performed along the centerline of the Main Trunk in about two hours (Fig. 2.1). The soundings began about 120 m upglacier from the terminus and extended to the uppermost Main Trunk. An additional 30-sounding transect across the Main Trunk was made and included soundings made, with some soundings made off the rock glacier on or near bedrock exposures. This transect crossed the Main Trunk about 150 m up from the terminus (Appendix 1). Figure 2.5 shows both a typical bedrock decay curve and a decay curve from the centerline transect.

TEM Interpretation

The observed decay curves in Figure 2.5 are, at first viewing, quite similar to each other. However, closer examination does indicate differences, and these represent variations in resistivity structure. Using the different curves in Figure 2.4a as a guide, it can be seen that the upper portion of the rock glacier is more resistive than the upper portion of the bedrock. The response curve on the rock glacier reaches the late-time I stage sooner than the bedrock response curve. The debris mantle and the ice-rock mélange of the rock glacier is likely contributing to this response, they are more resistive than the bedrock. Another distinct difference in these decay curves is the behavior of the magnetic field within the late-time II stage, as indicated by the arrow in Figure 2.5. At these times the bedrock curve rapidly becomes noisy, whereas the rock glacier curve

shows a slower and more noise-free decay. This slow and less noisy decay is observed on all decay curves from the centerline. It is an indicator that there is a conductive layer under the rock glacier that is not present in the bedrock.

These features are illuminated by smooth-model inversions, as shown in Figures 2.6a and b. In these inversions, the upper portion of the rock glacier is found to be more resistive than the upper part of the bedrock section. As suggested by the late-time II decay, there appears to be a conductive layer under the rock glacier ($< 50\ \Omega$ m) that is not present in the bedrock section. Elconin (1995) described the existence of a < 2 m-thick wet mud layer between the sole of the rock glacier and the bedrock. It was also reported that within the rock glacier mélange there was significant silt and clay (Elconin and LaChapelle, 1997). From these observations, it is quite likely that there exists a significant amount of wet, fine-grained material beneath the center of the rock glacier — similar to some glacial tills. This layer is illustrated in the TEM soundings by the conductive response observed at late times. It is unlikely that the conductive response is the result of a different bedrock found under the rock glacier than along its margins, although it may represent water-saturated bedrock under the rock glacier and not elsewhere. However, if this were the case, then this water must not be connected to the highly resistive water found in the pro-glacial stream (Table 1).

Comparison of the smooth-model rock glacier curve with that of the bedrock section shows that there is no bedrock signature beneath the basal conductive layer. This is likely because of increased eddy current (and induced magnetic field) diffusion and dissipation within the conductive till-like layer (via Eqn. 1).

The resistivity from the smooth-model inversion on the rock glacier is shown on a linear scale in Figure 2.6b, which more clearly indicates prominent changes in resistivity. We use the measured 58 m-thickness at the terminus to calibrate the model inversion of the sounding nearest the terminus. From this calibration we define the "depth-to-till" at the point where the resistivity decreases to ~900 Ω m (diagrammed in Fig. 2.6b).

There is also a change in resistivity at about 20 m depth. This value of 20 m is similar to that indicated by the seismic refraction, and to a lesser extent, the ice radar. However, this depth is much less well resolved by the TEM data. We note that the resolution of both this ~20 m discontinuity and the basal discontinuity is limited by the averaging effects of the geophysical smooth-model inversion, with possible depths of the basal layer indicated by the range shown by the box in this figure.

The smooth-model inversions for each of the ten soundings along the centerline are plotted along section in Figure 2.7a, where the location of each sounding is shown along the top axis. The data are then contoured to produce a pseudo-section along the rock glacier from about 120 m to 530 m up from the terminal face (located at 0 m). We interpret this as a longitudinal thickness profile for the rock glacier. This profile shows structure in the basal topography that is similar to that observed in the surface topography and marginal features. For example, Figure 2.1 shows the location of two snow-filled depressions along the margins, where we might expect a deeper rock glacier bed. There is a corresponding low in the pseudo-section at a longitudinal position of 340 m ('D' Fig. 2.7a), and a corresponding change in surface slope that is consistent with a rock glacier flowing over a dip in its bed.

We estimated the rock glacier thickness based on the 900 Ω m level in each of the ten centerline soundings following the calibrated signal (Fig. 2.6b). This leads to the longitudinal profile shown in Figure 2.7b. This depth corresponds to about the 900 Ω m contour in Figure 2.7a. From these data, and the slope of the valley walls, it is also possible to construct transverse cross-sections that conform to a reasonable channel geometry, as in Figure 2.7c.

The low-resistivity basal layer was also identified in the transverse TEM profile (Appendix 1). A localized anomaly was observed at depth over just the central part of the traverse. The anomaly was offset to the west of the centerline. This localized low-resistivity layer in the transverse section has a similar signature as that observed along the length of the longitudinal profile. This suggests that a wet till-like layer covers much of the central portion of the bedrock channel. The off-center location of this low resistivity layer is consistent with the observed asymmetrical wedge-shaped terminus geometry (Appendix 1).

CONCLUSIONS

We have investigated the geometry of Fireweed Rock Glacier using various geophysical techniques. Seismic, ice-radar and the DC resistivity methods were of limited value. Using seismic refraction we were able to resolve the thickness of the low velocity debris mantle (2-4 m). This is consistent with direct observations made by Elconin and LaChapelle (1997). Additionally, seismic refraction, and to a lesser extent,

ice-radar, suggests a discontinuity at about 18 to 28 m depth in the rock glacier. Such a discontinuity is also noted in the TEM results at about 20 m depth (Figs. 2.6 and 2.7). Analysis of the observed surface motion of this rock glacier (Chapter 3) indicates that this discontinuity may be a "shear plane" at depth, on and above which most of the glacier's motion occurs.

TEM methods effectively circumvent the debris mantle coupling problems that complicate other geophysical methods, and with TEM we were able to resolve the thickness of the rock glacier. Instrumental setup and data collection are efficient and require minimal time and power. Analysis requires care, but we were able to determine this thickness even with the inferred complex channel geometry. Calibrating this method with the terminal exposure of the rock glacier, we determined the thickness of the Main Trunk to be about 40-60 m. From these results it is possible to construct longitudinal and transverse cross sections that are consistent with the shape of the valley walls, marginal features and surface slopes. There is a prominent low-resistivity layer below the more resistive rock glacier, which we interpret to be a till-like layer. It is interesting that this layer probably enhances our ability to resolve the thickness because of its well-defined signature.

ACKNOWLEDGEMENTS

This study was supported by U.S. National Science Foundation grant #NSF-OPP98 06648. We would like to thank D. Rosenkrans and the National Park Service for

cooperation and support, and K. Zonge, S. MacInnes and S. Urquart (Zonge Engineering, Tucson) for their invaluable assistance with the TEM method and analysis. We appreciate the contributions of C. Bucki, L. Cox, P. Del Vecchio, R. Elconin, L. Goodman, W. Harrison, D. Mouldry, K. Smith, M. Truffer and E. Wescott. K-9 support was provided by Tazlina, Choly, Baxter, and McKenzie.

LITERATURE CITED

Costello D.P. 2000. Seismic and geomorphic investigations of Galena Creek Rock Glacier. Master's Thesis, University of Colorado, Boulder, Colorado.

Elconin, R.F. 1985. Internal composition, structure, and genesis of an active and well developed compound rock glacier, Wrangell Mountains, Alaska. Master's Thesis, Humboldt State University, Arcata, California.

Elconin, R.F. and E.R. LaChapelle. 1997. Flow and internal structure of a rock glacier. J, Glaciol., 43 (144), 238-244.

Evin, M., D. Fabre and P.G. Johnson. 1997. Electrical resistivity measurements on the rock glaciers of Grizzly Creek, St. Elias Mountains, Yukon. Permafrost Periglac. Process. 8. 179-189.

Fisch, W.Sr., W.Jr. Fisch and W. Haberli. 1977. Electrical resistivity soundings with long profiles on rock glaciers and moraines in the Alps of Switzerland. Zeitschrift für Gletscherkunde und Glazialgeologie, 13 (1/2), 239-260.

Haeberli, W. 1985. Creep of mountain permafrost: internal structure and flow of alpine rock glaciers. Mitteilungen der Versuchsanstalt für Wasserbau, Hydrologie und Glaziologie an der Eidgenössischen Technischen Hochschule (Zürich), Nr. 77.

Hauck, C., M. Guglielmin, K. Isaksen and D. Vonder Muhll. 2001. Applicability of frequency-domain and time-domain electromagnetic methods for mountain permafrost studies. Permafrost Periglac. Process. 12 (1), 39-52.

Hauck, C., 2001. Geophysical methods for detecting permafrost in high mountains. Mitteilungen der Versuchsanstalt für Wasserbau, Hydrologie und Glaziologie an der Eidgenössischen Technischen Hochschule (Zürich), Nr. 171.

Kaufman, A. A. 1979. Harmonic and transient fields on the surface of a two-layer medium: Geophysics, 44, 1208-1217.

Kaufman, A.A. and G.V. Keller. 1983. *Frequency and Transient Soundings*. Elsevier. New York. 695 p.

Keller, G.V. 1991. Rock and mineral properties: in Nabighian, M.N., Ed., *Electromagnetic Methods in Applied Geophysics*, Vol 2, Soc. Expl. Geophys., 13-51.

MacKevett, E.M. and J.G. Smith. 1972. Geologic Map of the McCarthy B-6 Quadrangle, Alaska: U.S. Geological Survey, GQ-1035, 1 sheet.

Nabighian, M.N. 1979. Quasi-static transient response of a conducting half-space — An approximate representation. Geophysics, 44, 1700-1705.

Nabighian, M.N. and J.C. Macnae. 1991. Time-domain electromagnetic prospecting methods: in Nabighian, M.N., Ed., Electromagnetic methods in applied geophysics, Vol 2, Application. Soc. Expl. Geophys., 427-478.

Petrenko, V.F. and R.W. Whitworth. 1999. *Physics of Ice*. Oxford University Press. New York. 373 p.

Vonder Mühll, D., C. Hauck, H. Gubler, R. McDonald and N. Russill. 2001. New geophysical methods of investigating the nature and distribution of mountain permafrost with special reference to radiometry techniques. Permafrost Periglac. Process. 12 (1), 27-38.

Ward S.H. and G.W. Hohmann. 1987. Electromagnetic Theory for Geophysical Applications: in Nabighian, M.N., Ed., *Electromagnetic Methods in Applied Geophysics*, Vol 1, Theory. Soc. Expl. Geophys., 131-311.

Sample	Resistivity (Ω m)
mudstone 1 (altered)	2024
mudstone 2	3532
igneous	3005
altered igneous 1	910
altered igneous 2	685
stream water	8500
glacier ice (temperate)	2.0×10^6 - 1.2×10^8

Table 2.1: Resistivities of rock glacier materials.

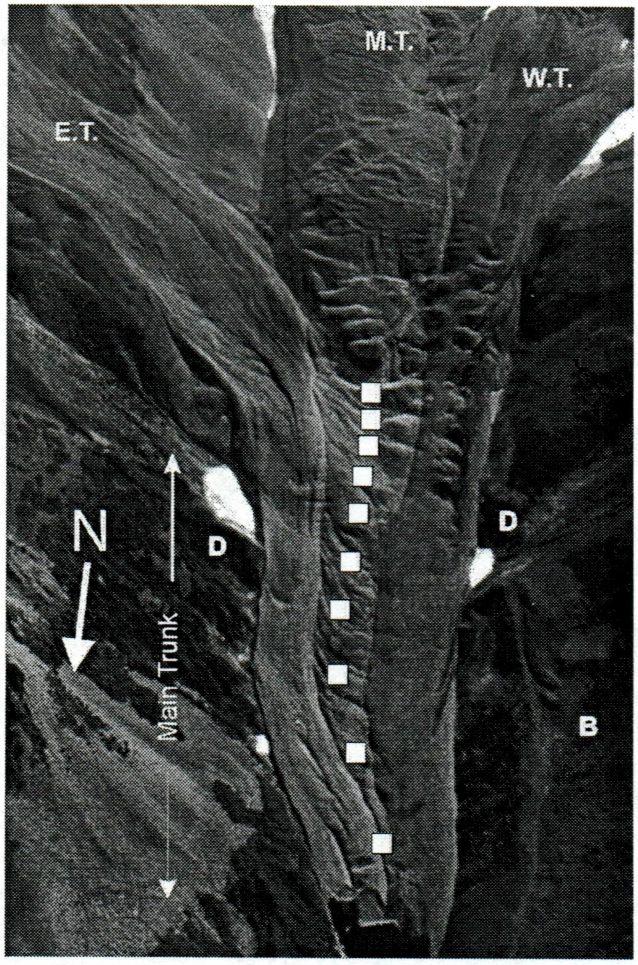

Fig. 2.1: Rock glacier overview and TEM sounding locations. Main Trunk of the rock glacier showing the East, Middle and West tributaries labeled with "E.T.", "M.T." and "W.T." White squares indicate approximate location of individual centerline NanoTEM soundings. The horizontal distance between each sounding is about 50 m. "**B**" is the location of the bedrock sounding. "**D**" marks the location of marginal, snow-filled depressions corresponding to detected subsurface topography of the rock glacier, about 340 m from terminus.

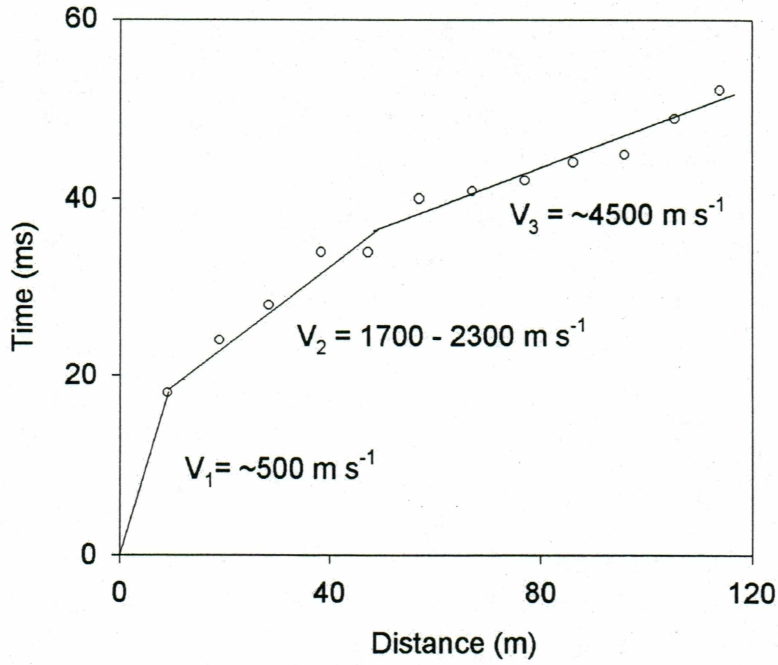

Fig. 2.2: Seismic refraction data. P-wave first arrival times from an array along the Main Trunk centerline. Layer 1 is the debris mantle, layer 2 and layer 3 may represent a discontinuity within the ice-rock mixture. V_i = (slope of linear segments)$^{-1}$

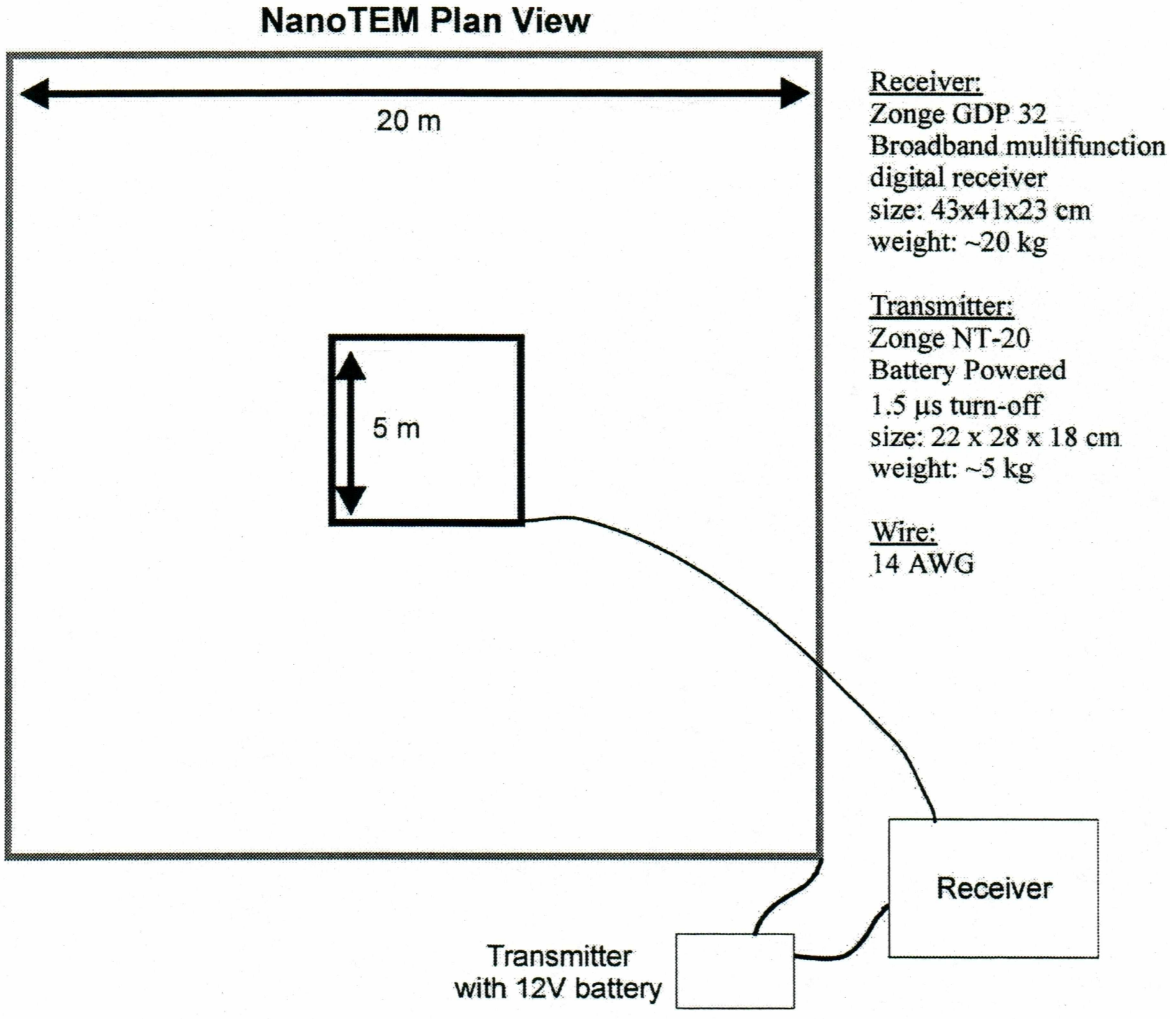

Fig. 2.3: TEM system description.

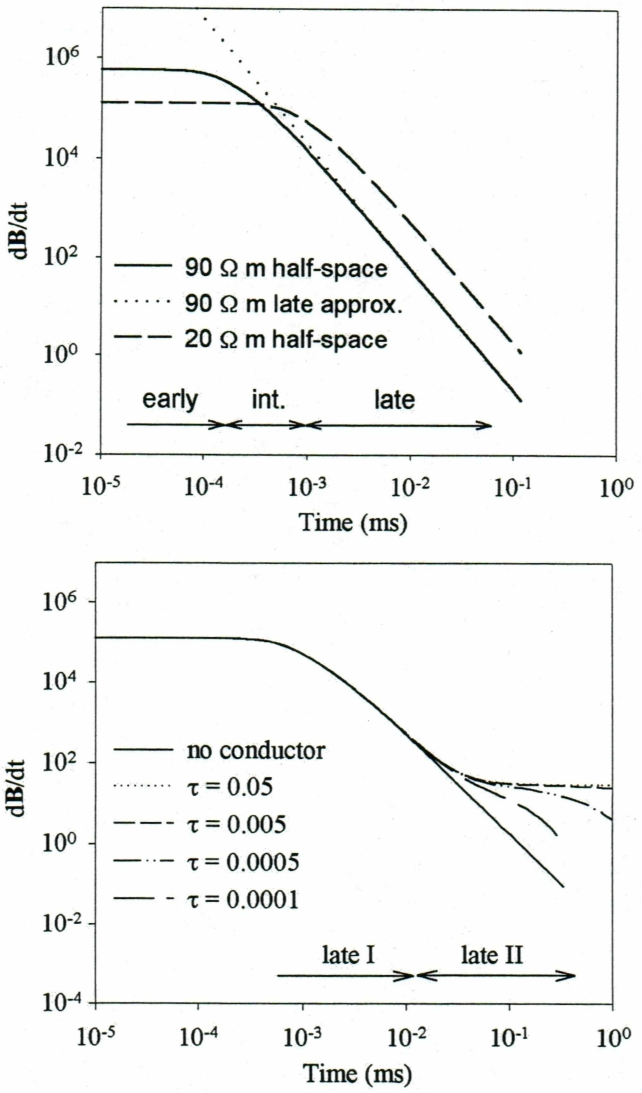

Fig. 2.4: Theoretical transient response. Time rate of change of the secondary magnetic field is measured (d**B**/dt) versus time from the shut-off of the primary magnetic field. a) Responses from two half spaces according to Equations (2) and (4), with an 11 m transmitter radius and current of 3.5 A. "early", "intermediate" and "late" correspond to decay stages and are shown for the 90 Ω m half-space. b) Complete response in the presence of a conductor. The superposition of Equations (2) and (6) is shown for various conductors buried in a half-space. Late-time is divided into late-time I and late-time II.

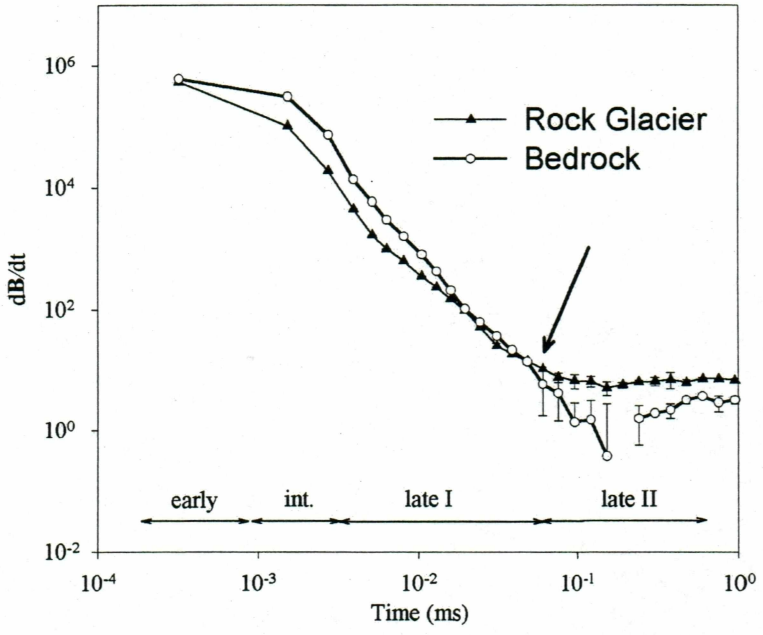

Fig. 2.5: Decay curves from the rock glacier centerline and the nearby bedrock. The relatively slow decay shown after the arrow on the rock glacier curve indicates a conductor under the rock glacier, most likely a saturated till. Error bars reflect the standard deviations of the stacked records in each case. Note that the bedrock curve has larger errors in late-time II.

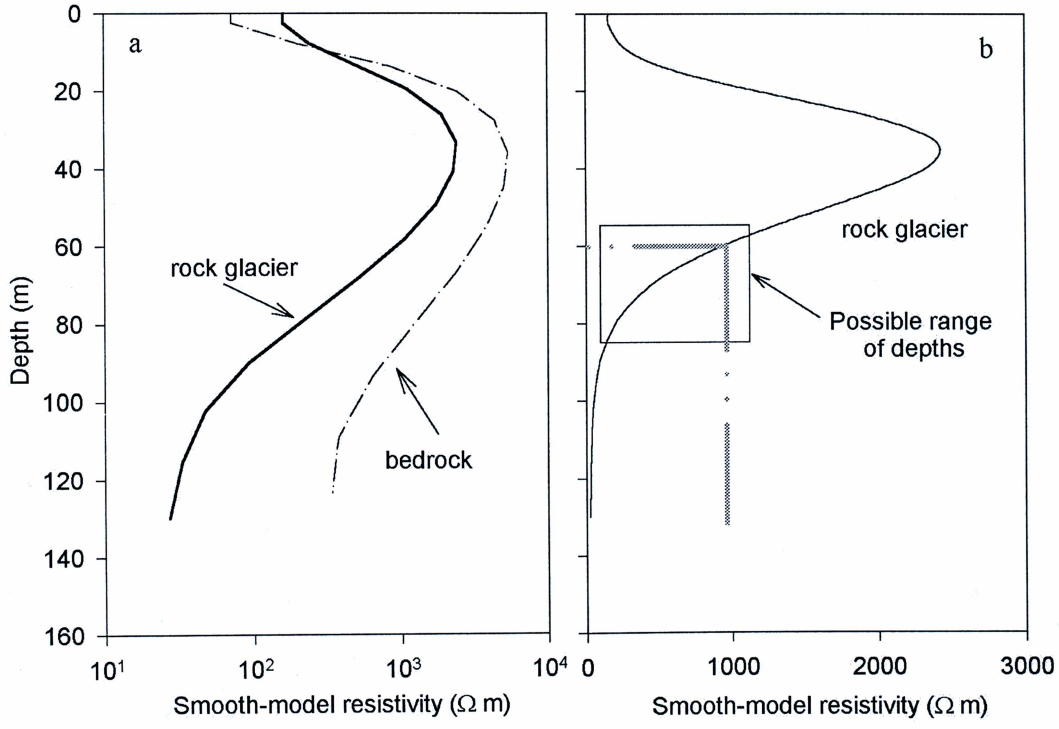

Fig. 2.6: Smooth-model resistivity example. Calculated resistivites from decay curves in Figure 2.5. a) logarithmic scale and b) linear scale.

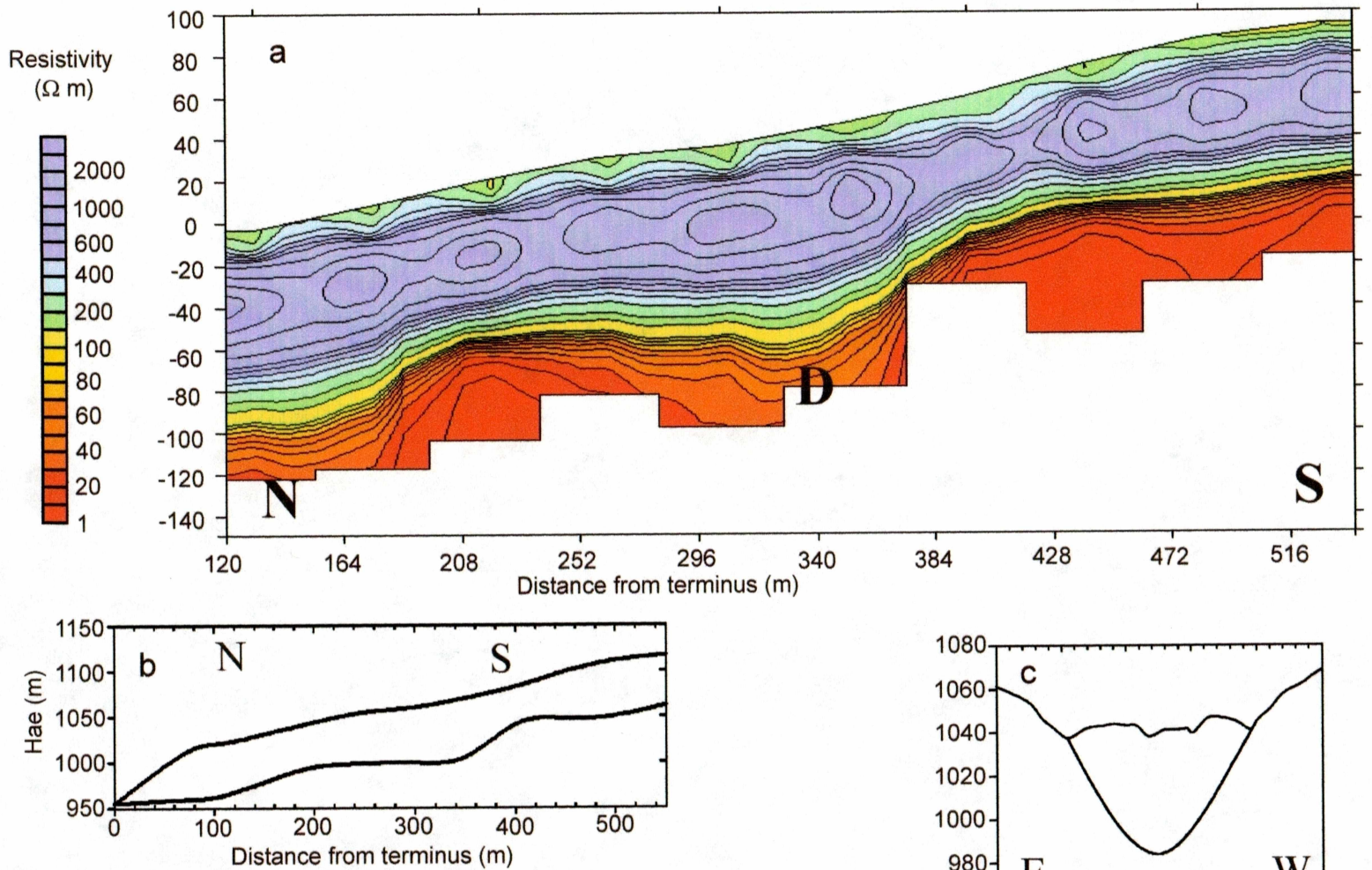

Fig. 7: TEM pseudo-section and rock glacier geometry. **(a)** NanoTEM smooth-model resistivity cross section, (b) and centerline profile determined from NanoTEM soundings and (c) transverse parabolic cross-section 170 m from terminus determined from surface topography and NanoTEM depths.

CHAPTER 3:

The Flow of Fireweed Rock Glacier, Alaska[1]

ABSTRACT

Fireweed Rock Glacier is a large rock glacier in southcentral Alaska. It flows relatively fast, with velocities up to 3.5 m a^{-1}, and exhibits both seasonal and annual variations, some of which are related to periodic terminus calving and increased rainfall. Our analysis reveals that motion is likely concentrated in a pseudo-rectangular channel within the larger parabolic channel with a "shear plane" at ~27 m depth. There is likely motion along the shear plane as well as internal deformation above it. We estimate that the ice-rock mélange is about two times softer than clean glacier ice. Prominent transverse ridges exist in an extensional flow field. Calving at the terminus is an important component of the mass balance.

[1] This chapter will be submitted to the Journal of Glaciology

INTRODUCTION

The internal structure and flow mechanisms of rock glaciers are poorly understood. They are composed of a mélange of ice and rock, where the rock debris ranges in of size from silt to medium-sized boulders. They are covered with an ice-free debris mantle a few meters thick, which inhibits or eliminates surface ablation as a component of mass balance. Rock glaciers are typically thin (<50 m), and they move relatively slowly, typically on the order of 1 m a^{-1}. While the rheology of the ice-rock mélange is likely to be different than that of clean glacier ice, we still might expect that, like ice glaciers, both internal deformation and motion at the bed govern their flow.

A rare glimpse into the internal structure of a rock glacier has been provided by the quasi-periodic calving of Fireweed Rock Glacier, Alaska (Elconin and LaChapelle, 1997). These authors found that the rock glacier was composed of a heterogeneous mixture of ice and rock, with several indicators of deformation. In addition, it has relatively high surface velocities (> 3m a^{-1}) compared to velocities commonly observed on most other rock glaciers. Here we describe observations of surface velocities and topography, and investigate the correlation among the calving, precipitation and velocity variations. We then analyze the velocities in order to estimate the nature and magnitude of basal motion and internal deformation. From these models and the observed flow we are able to estimate the rheological parameters of the rock glacier mélange.

DESCRIPTION OF FIREWEED ROCK GLACIER

Location and Overview

This rock glacier is situated in southcentral Alaska on the southern flank of the Wrangell Mountains (Fig. 3.1). It flows down a north-facing valley on Fireweed Mountain, and is the largest of 12 rock glaciers there. The valley that it occupies previously contained a small ice glacier as evident by the broader U-shaped valley and moraines near the terminus (Fig. 3.2). There are three tributaries that originate at elevations of 1400 to 1600 m and coalesce to form the Main Trunk, which terminates at 1000 m in a narrow, steep-sided valley. On the Main Trunk, v-shaped longitudinal furrows separate contributions from the tributaries (Fig. 3.1), and each tributary (and its contribution to the Main Trunk) is distinct in coloration due to different lithologies. We term these distinct contributions on the Main Trunk as a "flow" (Fig 3.2). The rock glacier exceeds 2 km in length from the head of the Middle Tributary to the terminus. The East Tributary is about 1350 m long from its head to the confluence with the Main Trunk and the Main Trunk flows for about 470 m (Fig. 3.1b) from the confluence of the East and Middle Tributaries to the break in slope at the terminus (the "terminus break"). This geometry is to be compared with that of some well-studied rock glaciers in the Alps, such as Murtél and Grüben in Switzerland (Haeberli, 1985; Haeberli and others, 1998), which are typically less than 1 km long and consist of a single flow extending onto a flat slope.

Fireweed Rock Glacier exists entirely below the regional equilibrium line altitude of nearby ice glaciers, which is ~1800 m above sea level as observed in late August 2000 and 2001. Semi-permanent snow patches, resulting from avalanche debris and shading, exist in all cirques and along the margin. The mean annual temperature is about -6° to -9 ° C, as estimated from temperatures measured in the nearby town of McCarthy (460 m elevation and 9 km to the southeast) with a lapse rate of 6 °C km^{-1}. In McCarthy, mean annual precipitation is 0.42 m and average snow depth during the winter is 0.35 m.

With geophysical exploration methods, especially transient electromagnetic ones, we determined the thickness of the Main Trunk of the rock glacier to be about 55 m (Fig 3.1). In addition to this depth-to-bedrock measurement, we observed a seismic and, to a lesser extent a resistivity, discontinuity ranging at about 15 m depth in the upper Middle Tributary to about 30 m in the Main Trunk (Chapter 2).

Tributaries and Debris Mantle

The rock debris mantle is composed of two main lithologies: a fine-grained felsic igneous rock and a fine-grained mudstone. Both occur in different states of hydrothermal alteration. On the East Tributary, the debris is composed of ~65% unaltered igneous rock and ~35% mudstone. On the Middle Tributary, it consists of about equal parts of the two unaltered rock types. The mantle of the West Tributary is composed of ~20% altered

mudstone and ~80% mostly altered igneous rock; this high percentage of altered rocks gives the West Tributary and flow a reddish hue.

Elconin and LaChapelle (1997) measured the thickness of the debris mantle on the Middle Tributary to be 0.7 to 1.2 m in moulin-like and bergschrund-like features, while at the terminus they found the mantle to be 2 to 3 m thick. Seismic soundings 90 m upglacier of the terminus indicate a debris mantle thickness of about 2.5 m (Chapter 2). This thickening of the debris mantle toward the terminus has been observed on other rock glaciers (Barsch, 1987).

Rocks of 0.1 to 0.6 m diameter make up the visible debris mantle; their average size decreases from the head to the terminus. Soils are nearly absent on the upper tributaries, but are more common on the Main Trunk, where they occur as a matrix between the blocks and in the furrows between the flows. A few small shrubs and grasses occur in these areas.

Surface Features

Much of the rock glacier has a convex transverse surface profile (Fig. 3.1c). This shape is most evident where there are no talus slopes draping onto the rock glacier's surface. In some areas where talus overlaps onto the surface, the surface is concave. However, in other areas where talus falls toward the rock glacier, a trough separates the rock glacier and the talus slope and does not appear to contribute to its mass balance.

But, in some years of our study, a few of these troughs have been completely filled with snow, making a smooth transition from the talus slope to the rock glacier. And possibly allowing avalanched rock debris to be deposited on the surface.

Transverse ridges exist on two of the tributaries, but unlike many rock glaciers (e.g. those studied by Kääb and others, 1998), they do not occur near the terminus. The most distinct set of these transverse ridges occurs on the upper West Tributary, while ridges in the Middle Tributary are small. There are also crevasse-like features ('C' in Fig. 3.2); the extent to which they penetrate below the debris mantle cover is unknown. The "crevasses" are associated with a steep area on the Middle Tributary (labeled I in Figs. 3.1 and 3.2). Above this steep section the crevasses are orientated similar to marginal shear crevasses on ice glaciers, which tend to intersect the valley walls at an angle of about 45° upglacier. The crevasses occur where the transverse surface is convex and a large, deep trough separates the surface of the rock glacier from the valley walls (Fig. 3.1). Within the steep section, crevasses are oriented perpendicular to flow, similar to those found above an icefall. Below the steep section, crevasse-like features are found along much of the Middle Flow, while along the West Flow the crevasse patterns smooth out below the steep section. The steep section of the East Tributary (II in Figs. 3.1 and 3.2) is smooth and does not have crevasses or ridges. On the lower 150 m of the East Flow, there is a set of longitudinal ridges and furrows ('B' in Fig. 3.2) associated with distinct internal structures that are exposed at the terminus during calving events.

Terminus Calving Events and Internal Structure

In 1993 the terminus calved and provided a complete transverse exposure of its internal structure (Elconin and LaChapelle, 1997). The calving event followed a period of heavy rainfall at the end of August. When first observed (1 Sept.) the terminus was overhanging and undercut by the proglacial stream. The calving and melt ablation of the exposed terminus caused a retreat of about 50 m. By September 1995, the terminus was completely draped by a steep slope of rock debris and it had advanced since the calving event.

From the exposure created during the 1993 calving event, Elconin and LaChapelle (1997) described the internal structure as a "consolidated mélange of ice and rock," with a bulk ice concentration greater than 50%. They concluded that the mélange is formed by the accumulation of ice and talus at the bases of the cirque headwalls. Photographs (e.g. Fig. 3.3) and descriptions of the terminus exposure show heterogeneous concentrations of ice and rock. An ice-rich region (~90% ice) exists at the terminus of the East Flow (Fig. 3.3b). The longitudinal ridges and furrows on the East Flow ('B' in Fig. 3.2) appear to be a surface expression of this ice-rich area, and anomalously large surface velocities exist there. The remainder of the East Flow contains 30-50% ice. At the terminus, the Middle Flow is largely overrun or displaced by the East Flow and, as a result, it contributes little to the exposed face. Where the Middle Flow outcropped, it had an ice concentration of about 30%. The West Flow contains about 50% ice. Elconin and LaChapelle (1997)

found thin layers of bubble-free and debris-free ice within the terminus face. They also found aligned debris clasts, foliation and elongated bubbles, all of which indicate deformation.

The terminus again calved after August 2000 and before May 2001, and we believe that it may calve regularly. This recent event may have occurred as early as September 2000, when there was a period of extreme rainfall — more than twice the precipitation than during the rain event prior to the 1993 calving. Rainfall in McCarthy over the seven-day period from 20-26 September 2000 was almost 13 cm, whereas in late August 1993, 5 cm of rain fell. The overall magnitude of the 1993 calving event was much larger than the 2001 event. However, we note that the over-steepened terminal face observed in September 2001 may cause additional calving over the following year.

Estimates based on observations made in August 2001 indicate that about 12,000 m^3 of material were removed from the snout as a result of calving. A talus apron skirted the bottom third of the terminus (Fig. 3.3a), but its volume was estimated to be only a fraction of the estimated calved material. The remainder of the calved material was melted or washed away by the proglacial stream. The timing of the calving event coincided with changes in surface velocity on the lower Main Trunk, as described in the following section.

SURFACE TOPOGRAPHY AND VELOCITY FIELD

Methods

The geometry of the rock glacier was determined by topographic surveys of the surface and by geophysical soundings (Chapter 2). A longitudinal section of the Main Trunk is shown in Figure 3.1d. In 1997 we established a survey network of four benchmarks (Fig. 3.4) using GPS methods. A theodolite and electronic distance meter were used for the surface and motion surveys. The centerline thickness of the Main Trunk of the rock glacier was determined to be 50 to 60 m using geophysical soundings, and the channel shape can be approximated as a parabola (Fig. 3.1c).

Over 300 positions on the 0.83 km^2 total surface area were surveyed to define the surface topography and margins. This included longitudinal profiles of each of the tributaries with a position measured every 50 m along flow. The uncertainties for these measurements are about 0.3 m in both the horizontal and vertical. More detailed surveys were made of the terminus break and of the transverse ridges on the West Tributary.

Velocity markers were positioned in four transverse profiles on the Main Trunk (Profiles A-D in Fig. 3.4b), and throughout the tributaries. On the tributaries, many of the markers were placed along the longitudinal profile (Fig. 3.4). The markers were 60 cm sections of steel-reinforcement bar ("rebar") that were set into the debris layer so that only ~3-15 cm projected above the rough surface. Stability of the markers was good and minimal tilting occurred over the measurement period. Limited velocity surveys began in

1997, followed by more complete surveys in the summers of 1998 to 2001. Long-term average velocities were calculated over the two-year period from July 1999 to August 2001. To detect seasonal variations in flow, surveys were made in late June/early July and then again in late August/early September of both 1999 and 2000. Surveys made in 1999 and later have estimated horizontal and vertical position errors of about 0.02 m and 0.04 m on the Main Trunk, respectively, and 0.04 m and 0.07 m on the tributaries. Estimated errors for the pre-1999 surveys are about twice these values.

Topography, Slopes, and Ridges

The elevation along each longitudinal profiles shown in Figure 3.4, is shown in Figure 3.5a. The local surface slope at each of these markers was calculated from the surface elevations over a longitudinal distance of 100 m. The uncertainty of these local surface slopes is about 0.5°. Along the centerlines of the Main Trunk and tributaries, the surface slope ranges from about 3° to 27°; the steepest sections are labeled 'I' and 'II' in Figures 3.1 and 3.2. (This does not include the terminus front or the margins that dip toward the valley walls, which have slopes of about 40°.) The average slope of the Main Trunk is about 13°; the Middle Tributary, inclusive of the steep section, averages about 16°, and both the East and West tributaries average 14°.

Formation of the transverse ridges on the West Tributary begins upglacier of our uppermost velocity marker there (Fig. 3.4). The uppermost ridges have a peak to trough

amplitude of < 1 m, which increases for some distance downglacier. The amplitude then decreases until the ridges disappear ~500 m downglacier (roughly 800 years) of their inception. Detailed surveys of the middle section of these transverse ridges were carried out in July 1999 and August 2001. The transect began at the uppermost large transverse ridge and followed the line of the velocity markers along the tributary. Surface elevations were determined at about 10 m intervals, approximately corresponding to the crest and trough of each ridge (Fig. 3.6). Within the surveyed section there were two distinct ridge amplitudes, one about 2 m and the other about 1 m. The wavelength increases from about 20 m near the upper extent of the large ridges to about 50 m at the downglacier end of the ridges. Comparison of the surveys in 1999 with those in 2001 shows no discernable change in their position, so with the resolution of our surveys it is impossible to determine if the transverse ridges are advecting downglacier or their location has remained fixed in space.

The Terminus Front and Terminus Break

In July 1999, a marker (TP) was set into the debris mantle on the West Flow about 3 m upglacier of the terminus break (Figs. 3.3a and 3.4b). From this location, the average slope of the terminus front was measured to be about 38° in 1999 and 2000. By August 2001, calving had removed material between the marker and the old terminus break, and

the average slope of the calved terminus was 40°. However, following calving the upper 20 m was nearly vertical with a lower angled talus apron below (Fig. 3.3a).

The transverse position of the terminus break was measured from 1999 to 2001 (Fig. 3.7). From 2000 to 2001 the break retreated by calving in the central portion and it advanced somewhat near the margins. Some material was removed from the marginal areas by calving, but there was still a net advance there. Removal of material by the calving was evident everywhere along the terminus, with exposed ice, fresh surfaces, and the close-to-vertical face (Fig. 3.3a). The largest calving retreat was in the East Flow, where Elconin and LaChapelle (1997) described the ice-rich region.

The Surface Velocity Field

Horizontal surface velocities (1999 to 2001 averages) are less than 0.5 m a^{-1} on the upper tributaries of the rock glacier and increase on the Main Trunk to a maximum of 3.8 m a^{-1} as measured 80 meters above the terminus on the East Flow (Figs. 3.4 and 3.5). At the terminus break of the West Flow, the speed was about 4 m a^{-1} (Fig. 3.7). (The error in these two-year velocities is about 0.03 m a^{-1}.) Analysis of air photos taken in 1957, 1970 and 1994 indicates that surface velocities with this order of magnitude have persisted for several decades. These are exceptional velocities for a rock glacier; typical velocities are ~1 m a^{-1} or less (Haeberli, 1985; Barsch, 1987; Konrad and others, 1999). The steep sections of the East and Middle Tributaries have somewhat higher velocities

than the other tributaries, but in general there appears to be no direct correlation between surface slope and surface velocity (compare Figs. 3.5a and b). For example, in the steep section I the slope is 27° and the speed is 1.5 m a^{-1}, while just above this steep section, where the local slope is 17°, velocities are about 2.0 m a^{-1}.

Surface Velocity Field of the Main Trunk

The magnitude of the velocity increases by as much as 1.5 m a^{-1} from Profile B to Profile A, a distance of 100 m (Fig. 5b). The velocity profile at A is asymmetric (Fig. 3.8a). The largest velocities on the rock glacier (except for at marker TP) are on the East Flow, where they are associated with the ice-rich region identified in the calving front. The velocity vectors in this ice-rich region are oriented about 10° more westward than the general channel direction, and the flow appears to displace (or override) the ice-poor part of the rock glacier (Fig. 3.2 and 3.4b).

The transverse velocity pattern at Profile B is more symmetric, but it is plug-like in shape (Fig. 3.8b), having high marginal shear strain rates. The velocities measured close to the margins are about 0.6 m a^{-1}; these give effective transverse gradients in velocity of about 0.3 a^{-1} near the east margin and 0.1 a^{-1} at the west margin, assuming there is no marginal "sliding". Similarly, the near-margin transverse velocity gradients at Profile A are about 0.2 a^{-1}. Profiles C and D show similar patterns as those found at Profile B, including the nearly plug-like flow.

Velocity Patterns in the Transverse Ridges

The central flowline and the line of our velocity markers on the West Tributary are roughly normal to the transverse ridges there. The surface velocity increases from the upglacier end (0.35 m a^{-1}) to the downglacier end (0.41 m a^{-1}) of our longitudinal transect, as shown in Figure 3.6. This positive longitudinal velocity gradient through the ridges corresponds to an increase in amplitude and in wavelength of the ridges. Downglacier of this, where the transverse ridges vanish, velocities continue to increase (Fig 3.4a). Unfortunately, our velocity marker coverage does not extend upglacier into the upper-most ridges.

Longitudinal Strain Rates

Longitudinal strain rates were estimated from the measured two-year average velocities over a longitudinal separation Δx between markers:

$$\varepsilon_x = \frac{\Delta v}{\Delta x} \tag{3.1}$$

Figure 3.5c shows the longitudinal strain rate along the central flowlines. They are small, generally about 0.002 a^{-1}, but increase to 0.008 a^{-1} near some of the steeper sections. These are about an order of magnitude less than typical strain rates on temperate valley

glaciers, but are similar to those measured on McCall Glacier in arctic Alaska, where they correspond to a low mass- balance gradient and mass flux (Rabus and Echelmeyer, 1997).

The pattern of strain rate is unlike that expected on an ice glacier, where the accumulation area is generally extending, the ablation area is compressive and the rate of extension is often high where the surface slopes are high. On Fireweed Rock Glacier, the strain rates increase above steep sections I and II and decrease within them. The strain rates are negative (compressive) at the base of the steep section (I) of the Middle Tributary, as expected, but they are positive below steep section II of the East Tributary. Strain rates increase within the narrowing Main Trunk between profiles B and A. The largest longitudinal strain rates of about 0.015 a^{-1} were measured on the West Flow near Profile A and marker TP. As noted, the flow is slightly extending along the transverse ridges of the West Tributary. However, there are similar extending strain rates on the East Tributary, where no transverse ridges exist.

Seasonal Variations

Motion surveys indicate that there is temporal variability in velocity at both seasonal and annual time scales. Figure 3.9 shows the two-year average annual velocity (thick line), along with velocities measured over shorter time intervals. The velocity variations are to be compared with their estimated errors over the 2000 to 2001 interval (~0.03 m a^{-1}) and over the shorter summer intervals (~0.15 m a^{-1}). The velocities in

summer 1999 were less than the two-year average by 40% at Profile A, 30% at Profile B and 13% at Profiles C and D. Velocities during the calving year from July 2000 to August 2001 were higher than average, especially at Profile A. After calving, velocities were largest on the East Flow. At Profile A velocities were as much as 1.2 m a^{-1} above the two-year average, and at B they were about 0.7 m a^{-1} above the average.

Strain rates also exhibit temporal variability. For example, in the lowermost 100 m of the East Flow, strain rates were especially high (0.05 a^{-1}) over the 2000-2001 period, being twice those measured over the previous three years (0.02 a^{-1}).

ANALYSIS OF SURFACE VELOCITIES AND CALVING

Precipitation, Velocity, and Calving

Precipitation records from 1987 to 2001 for McCarthy were obtained from the National Climate Data Center. The average annual precipitation over this interval was about 42 cm per year, and the three years with the highest recorded precipitation were 1988, 1993 and 2000.

Although our data are limited, there appears to be a correlation between times of increased precipitation and both velocity changes on the Main Trunk and calving at the terminus (Fig. 3.10, terminus status and velocity in 1988 are unknown). Similar correlations among velocity, calving and precipitation have been observed on tidewater glaciers (O'Neel and others, in press). The highest annual velocities measured at Profile

A correspond to those years having calving events, and the elevated velocities measured in the two years following the 1993 calving are likely associated with that event. It is inferred that velocities remained high while the terminus advanced into its pre-calved geometry. After calving, a longitudinal force imbalance exists at the unsupported face, providing an additional "pulling" force on the nearby portion of the rock glacier, analogous to the Jakobshavns Effect proposed by Hughes (1986) for tidewater glaciers. As the valley fills in and the terminus returns to its sloping, non-calved geometry (e.g. 1996 to 2000), longitudinal stress gradients near the terminus decrease, and the near-terminus velocities decrease.

Both the calving event in 1993 and that in 2001 were associated with periods of high rainfall, and an accompanying period of larger-than-normal velocities. Thus, increased precipitation, particularly large rainfall events, likely promotes calving, and this calving affects the surface velocity near the terminus. Of course, we would also expect that the terminus must build back up to some given geometry before it can again calve. This scenario is reasonable, but the limited resolution and coverage of our dataset does not preclude other possibilities.

Velocities in the West Tributary Transverse Ridges

The observed amplitude patterns on the transverse ridges of the West Tributary is similar to those patterns described by Kääb and others (1998) for formation, growth, and

decay of transverse ridges. However, the observed (but poorly resolved) weakly extensional flow regime (0.0003 a^{-1}; errors ±0.0004 a^{-1}) within the large amplitude ridges is contradictory to their observations. If we make the reasonable assumptions that the accumulation of material within the ridges is zero and that channel geometry does not vary, then the extensional flow should indicate thinning of the ridges. The velocity transect may be sub-parallel to a longitudinal axis of the ridges, in which case our observed flow would then be one of apparent extension. Our measurements lack the detail required to resolve these contradictory results.

Basal Motion and Deformation

The plug-like velocity profiles indicate that there are two contributions to the surface velocity, one from internal deformation (u_d) and one from motion along basal and marginal interfaces (u_{bed}). As already noted, Elconin and LaChapelle (1997) observed features that indicate deformation of the ice-rock mélange. In addition, temporal variations in the velocities strongly suggest a basal component of flow. Assuming that sliding or basal motion is the same everywhere across the bed and extrapolating the observed velocities at Profile A to the margins, which suggests that $u_d \approx 2$ m a^{-1} and $u_{bed} \approx 1$ m a^{-1}. Similarly, at Profile B, we estimate $u_d \approx 1.2$ m a^{-1} and $u_{bed} \approx 0.6$ m a^{-1}. Flow models discussed next provide some further insight into these two contributions.

Channel Geometry, Flow Models, and Rheology

The internal deformation of both ice glaciers (Paterson, 1994) and permafrost (Andersland and Ladanyi, 1994) is often described in terms of a power law rheology. For simple shear in a vertical plane, with x aligned parallel to flow and y positive upward, we have

$$\dot{\varepsilon}_{xy} = A\tau_{xy}^{n} \tag{3.2a}$$

where τ_{xy} is the shear stress, $\dot{\varepsilon}_{xy}$ the strain rate, and A is the flow law parameter, which can vary with temperature, debris content and impurities. The flow law exponent, n, is typically less than or equal to 5 for permafrost, and $n \leq 3$ is often used for clean glacier ice.

The calculation of shear stress for a rock glacier is complicated by the additional mass of the debris mantle, and by the often-unknown density of the mélange. For a two layer rock glacier with a deforming core of average thickness h and density ρ_c, and an overlying debris mantle of thickness d and density ρ_m, we have, at the bed

$$\tau_{xy}(bed) = fg(\rho_c h + \rho_m d)\sin\alpha \tag{3.2b}$$

where α is an appropriately averaged surface slope, g is the gravitational acceleration and f is a channel shape factor. Assuming the debris mantle rides passively on top of the deforming core (Kaufman, 1998), Equations 3.2a and 3.2b lead to a centerline surface velocity of

$$u_d = \frac{2A(f\rho_c g \sin\alpha)^n}{(n+1)}\left[\left[h+\frac{\rho_m}{\rho_c}d\right]^{n+1} - \left[\frac{\rho_m}{\rho_c}d\right]^{n+1}\right] \qquad (3.3)$$

(Konrad and others†, 1999). For $d << h$, the last term can be ignored. Here we take ρ_m to be about 2200 kg m^{-3} by assuming the mantle is composed of rock debris having a density of about 2800 kg m^{-3} and about 20% air space. Likewise, we estimate ρ_c to be about 1850 kg m^{-3}, by assuming equal volumes of ice and rock debris. With Equation 3.2b we calculate the basal shear stress (τ_{xy}) to be about 0.9 bars.

How the flow law parameter of ice varies with debris content is poorly understood; as a result, we must make *a priori* assumptions about A within the rock glacier. First, we assume that A is constant with depth and take $u_{bed} = 0$. At Profile B, u_d=1.8 m a^{-1}, h = 58 m, d = 2 m (Chapter 2), $\alpha = 9°$, and $f = 0.55$ for an assumed parabolic geometry (width = 158 m). From Equation 3.3 with $n = 3$, we find $A = 0.14$ a^{-1} bar^{-3}. This is about the same value found for temperate ice (e.g. Hooke, 1981; Truffer and others, 2001). However, this conclusion is based on the assumption that there is no basal or marginal motion, contrary to the observed plug-flow, as discussed in the previous section.

Velocity Profile and Channel Geometries

The analysis based on Equation 3.3 is limited to the centerline velocity.

---

† In Konrad and others (1999) the last term of this formula is incorrect, but in Konrad and others (2000) it has been corrected. The shape factor is not included in either version, and it is incorrectly applied to non-centerline surface velocities in the first version.

Information on flow mechanisms can also be obtained from the shape of a transverse velocity profile. Nye (1965) calculated the deformational velocity profiles of a glacier in various channel shapes, and Echelmeyer (1983) extended this analysis to various values of n. Here we compare the results of Echelmeyer (1983), scaled to the observed centerline velocity, with the velocity at Profile B (Fig. 3.11a). For any reasonable n (with constant A), the fit of parabolic channel flow to the observed velocities is poor as long as we assume no basal motion.

We can include basal motion by adding u_d and u_{bed} directly, although we acknowledge that this direct addition is likely more complicated because of stress transfer and the non-linear rheology expressed by Equation 3.2 (Truffer and others, 2001). Assuming a parabolic channel at B, with h = 58 m, and using u_d = 1.2 m a^{-1} and u_{bed} = 0.6 m a^{-1}, we find a flow law parameter of A = 0.08 a^{-1} bar^{-3}. This is about half that of temperate ice. However, the predicted velocity profile does not match the shape of the observed profile (Fig. 3.11b). Additional modeling shows that no assumed parabolic geometry with the measured centerline depth can reproduce the observed velocity pattern at Profile B — for any reasonable values of A, n and u_{bed}.

These models assume that deformation occurs throughout the rock glacier mélange in a channel geometry that is approximately parabolic. However, we note that the geophysical soundings on this rock glacier indicate a seismic discontinuity at 15 to 30 m depth. Also, observations at Murtél and Pontresina-Schafberg rock glaciers in

Switzerland indicate that all of the deformation is concentrated at (and possibly above) a shear horizon within the mélange (Haeberli and others, 1998; Hoelzle and others, 1998). Following these observations, we consider models with localized deformation at and above a plane at some depth in a parabolic channel of centerline depth 58 m. To simplify the computations, we assume that deformation is limited to the rectangular sub-section of the channel so defined, with "sliding" around its perimeter. We considered rectangular channels (Nye, 1965) with depths ranging from 58 m to 10 m and $n = 3$. (Of course, a 58 m-deep rectangular channel is unreasonable, given the projected shape of the valley walls.) We find that the fit for a rectangular sub-section with no sliding is still poor (Fig. 3.11c). A reasonable fit to the observed velocity profile arises by assuming a 27 m-deep rectangular subsection ($f = 0.87$) with $u_{bed} = 0.6$ m a^{-1} and $u_d = 1.2$ m a^{-1} (Fig. 3.11d). However, we note that this model is not unique. The value for A required to fit the observed surface velocity is 0.26 a^{-1} bar^{-3}. This is roughly two times softer than clean temperate ice.

Thus, the geophysical observations and the observed velocity profile suggest that there is a quasi-rectangular core that deforms more easily than clean ice, and that there is a zone of localized deformation at the base and sides of this core.

Longitudinal Stress Gradients and the Flow Law Parameter

Variations in glacier geometry, such as those shown in Figure 3.1, produce longitudinal stress gradients that influence the motion of a rock glacier. Following Kamb and

Echelmeyer (1986), we can approximately account for longitudinal stress gradients by an appropriate longitudinal average of slope, thickness and shape factor. These authors show that the centerline velocity in a non-parallel-sided channel is given by an exponentially-weighted average:

$$u_d(x) = u_d^0 + \frac{u_d^0}{2l}\int_0^L \Delta \ln(\alpha^n f^n h^{n+1}) \exp(-|s-x|/l)ds \qquad (3.4)$$

where u_d^0 is the velocity calculated for an average parallel sided reference state and Δ denotes the difference between reference state and the actual geometry at a longitudinal position s along the glacier. L is the length of the glacier and l is the longitudinal coupling length, which is about two times the ice thickness for glaciers with longitudinal surface strain rates on the order of 0.01 to 0.05 a^{-1}. Given the relatively small strain rates we observed near Profile B, we use a coupling length of about 4h (Kamb and Echelmeyer, 1986; l=230 m in this case). To determine an estimate of the flow law parameter (A) for the rock glacier mélange, we combine Equations 3.3 and 3.4 to give

$$A(x) = A_0\left(1 + \frac{1}{K}\int_0^L \Delta \ln(\alpha^n f^n h^{n+1}) \exp(-|s-x|/l)ds\right)^{-1} \qquad (3.5)$$

where A_0 is the flow law parameter calculated without longitudinal averaging from Equation 3.3 . An appropriate scaling factor of the exponential weighting function, K, is required because we cannot extend the analysis out to | s - x| = 2l, due to the limited length of our dataset.

We find that the effect of including these longitudinal stress gradients in each of the models discussed (Figs. 3.12a - d) is to decrease the value of A required to match the observed centerline speed by about 10%. For the rectangular subsection model, we assume that the depth of the subsection is constant along the length of the Main Trunk. (It should be noted that because of the longitudinal coupling length imposed on our limited data set, we are able to include only about 50% of the theoretical effects of the longitudinal stress gradients.) With this correction we find that the stiffness of the mélange in the best fit model (a 27 m deep rectangular subsection with 0.6 m a^{-1} sliding) is 0.27 bar^{-3} a^{-1}. This is roughly 2.5 times softer than clean temperate ice (A = 0.1 bar^{-3} a^{-1}; Truffer and others, 2001; Hooke and others 1981[‡]).

Rock glacier mélange may be similar to ice-rock mixtures in permafrost (Andersland and Ladanyi, 1994) and to the debris-laden ice found at the base of ice glaciers. The manner in which the rock debris influences the rheology of ice is poorly understood and observations regarding its rheology conflict. Laboratory studies have shown that weakening of ice occurs when debris concentrations are high (>70%), while at lower concentrations the mélange is stiffened with respect to ice (Hooke and others, 1972; Nickling and Bennet, 1984). The mechanism often suggested explaining stiffening by debris is that, for most concentrations, the debris particles collide and act as pinning points, thus strengthening the mélange.

[‡] Note that these authors and others found that the best value for the flow law parameter of temperate ice is about half that recommended by Paterson, 1994, p. 97.

In-situ studies indicate that debris concentrations of 25% - 60% result in significant softening of ice-rock mixtures (Echelmeyer and Wang, 1987; Cohen, 2000). Also, extrapolation of in-situ permafrost studies to the temperature and stress conditions within glaciers indicates softening with respect to clean ice. A mechanism for this softening has been suggested by Echelmeyer and Wang (1987), in which interfacial water at the debris-ice contacts allows slip at each debris particle, lowering the effective viscosity. Cohen's observations of the water content, fabric and deformation of debris-laden ice (2000) support this idea. This mechanism can also lead to shear planes in heavily debris-laden ice, as observed by Echelmeyer and Wang (1987). Our inferred softening of rock glacier mélange at Profile B is consistent with these later observations. If these increased values of A are indeed typical of rock glacier mélanges, then we expect that rock glaciers would have higher surface velocities than ice glaciers of similar geometry and basal shear stress. However, we must note that the non-uniqueness of our best-fit model, with an interplay between the depth to the shear plane, u_{bed}, mélange density and A limits these conclusions.

Mass Balance of Fireweed Rock Glacier

For ice glaciers, mass balance and longitudinal changes in channel geometry control the longitudinal strain rate and emergence velocity (Paterson, 1994). On this rock glacier, the patterns of longitudinal strain rate along the rock glacier (Fig. 3.5c), and

patterns of the measured emergence velocity (Appendix) are different than those typically observed on ice glaciers. Thus we might expect that the mass balance distribution of the rock glacier is different than that of an ice glacier in both the sources and distribution of accumulation, and the insulating effects of the debris mantle. On a rock glacier, accumulation may not be limited to talus cones, as surface water (meteoric and/or melt) can freeze below the debris mantle along the length of the rock glacier and add ice to the mélange. Near-surface ablation is severely limited by the debris mantle over the entire length of the rock glacier. This distribution of mass balance can support the convergent flow observed at the terminus of Fireweed Rock Glacier, which should be compared to ice glaciers that typically exhibit divergent flow as a response to ablation.

At the terminus, calving (and calving-induced melt ablation, Elconin and LaChapelle, 1997) is a significant mechanism of mass loss that does not exist on other rock glaciers. As a result, other rock glaciers are likely much further from a steady-state length than Fireweed Rock Glacier, and are subject to continuous advance (Konrad and Humphrey, 2001). We suggest that Fireweed Rock Glacier is subject to periodic calving. The time to the next calving event can be estimated using the flux through the rectangular section at Profile B (~5700 m^3 a^{-1}), and assuming that the terminus geometry (and glacier length) that existed prior to September 2000 is necessary (but not sufficient) for calving to occur. This calculation indicates that by Fall 2003 the glacier may be primed for calving once again. Of course, a rainfall event of sufficient magnitude is likely required

some time after that as well.

The mass contribution from the talus cones may also be investigated by considering the ice flux at Profile B. We assume that any accumulation from the freezing of surface-water under the debris mantle is small, and that the rock glacier is not changing in time. From air photos, we estimate that the area of talus cones in contact with the rock glacier surface (those with accumulation potential) is roughly 100,000 m^2. Based on our ice and rock flux estimate at Profile B (~5700 m^3 a^{-1}) and our assumption that ablation is very small, this indicates that the annual average accumulation over the area of the talus cones is about 0.057 m a^{-1}. Any surface water freezing would reduce this accumulation rate, as would any thinning at Profile B.

CONCLUSIONS

The flow of Fireweed Rock Glacier is similar that of an ice glacier in many ways, yet there are distinct differences. We have observed strong evidence of temporal variability, motion along a basal interface, and internal deformation. However, the shape of the transverse velocity profile indicates that most of the motion occurs on and above a shear plane. This shear plane is situated about halfway down into the rock glacier cross-section. At least one third of the motion is contributed by slip (localized deformation) on this plane and the remainder can be accounted for by internal deformation of the mélange. Thus, the effective channel shape is best modeled by a rectangular subsection about 27 m

deep in a parabolic channel with a 58 m centerline depth. Our best-fit model, which is necessarily non-unique in both the depth of the shear plane and the rheological parameters of the mélange (but constrained by reasonable geometries), implies that the ice-rock mélange is about 2.5 times softer than clean ice. This is consistent with the observations of Echelmeyer and Wang (1987) and Cohen (2000). It is noteworthy that anomalous geophysical findings described in Chapter 2 are consistent with the presence of a shear plane at about 27 m depth, and that such a flow discontinuity has been observed on other rock glaciers (e.g. Haeberli and others, 1996; Hoelzle and others, 1996).

We note, however, that this model does not explain the observed velocity patterns at Profile A, where there appears to be enhanced deformation in the ice-rich region relative to adjacent ice-poor regions. A possible explanation for this behavior is that enhanced basal motion may occur below this ice-rich flow as it overrides and displaces the Middle Flow near the terminus. This is suggested by the anomalous flow vectors on the east half of Profile A (Fig. 3.4), which are directed 10° more westward than expected for channel convergence.

Our analyses also show that longitudinal stress gradients, the shape of the channel (for which $f < 1$), the increased density of the rock glacier material, and the mass of the debris mantle all significantly affect the flow of a rock glacier. It has been suggested that changes in mélange temperature may lead to seasonal or annual velocity variations, such

as those we observed, through variations in the flow law parameter. However, such temperature variations beneath a thick debris layer are likely to be small (Harris and Pedersen, 1998) and insufficient to cause recognizable variations in stiffness of the core of this rock glacier. We conclude that hydraulic conditions — both englacial and subglacial — likely contribute to short-term temporal variations of rock glacier flow, as they do in ice glaciers.

There appears to be a correlation among near-terminus temporal velocity variations, calving, and precipitation. Our data show that large rainfall events may lead to terminus calving, if the terminus geometry is favorable. This in turn enhances flow near the terminus because of an increase in longitudinal stress gradients caused by the steep, unsupported calving face, similar to the Jakobshavns Effect proposed for tidewater glaciers (Hughes, 1986). The subsequent flow into the constricted valley and a less steep terminal slope reduces this longitudinal force imbalance with time. The calving of this rock glacier is also an important mechanism of mass loss that is not generally found on other rock glaciers.

The morphology of the transverse ridges in the West Tributary of Fireweed Rock Glacier is similar to that described by Kääb and others (1998), with an increase in amplitude followed by decrease. However, our observations indicate that these ridges exist in a region of slight extensional (or at least not compressive) flow, which is not consistent with the strain field of the ridges they describe. Further measurements of

velocity and strain rates are required to better document the mechanisms for transverse ridge formation.

ACKNOWLEDGEMENTS

This study was supported by U.S. National Science Foundation grant #NSF-OPP98 06648. We would like to thank D. Rosenkrans and the National Park Service for cooperation and support. We appreciate the contributions of C. Bucki, L. Cox, P. Del Vecchio, R. Elconin, L. Goodman, W. Harrison, D. Mouldry, K. Smith, and M. Truffer. K-9 support was provided by Tazlina, Choly, Baxter, and McKenzie.

LITERATURE CITED

Andersland, O.B., B. Ladanyi. 1984. *An Introduction to Frozen Ground Engineering*. Chapman and Hall. New York.

Barsch, D. 1987. The problem of the ice-cored rock glacier. In: Giardino, J.R., Shroder, J.F.Jr., and Vitek, J.D., Eds. *Rock Glaciers*. Allen and Unwin. Boston. 45-53.

Cohen, D. 2000. Rheology of ice at the bed of Engabreen, Norway. J. Glaciol., 46 (155), 611-621.

Echelmeyer, K.A. 1983. Response of Blue Glacier to a perturbation in ice thickness: theory and observation. Doctoral Thesis, California Institute of Technology, Pasadena California.

Echelmeyer, K.A. and Z. Wang. 1987. Direct observation of basal sliding and deformation of basal drift at sub-freezing temperatures. J. Glaciol., 33 (113), 83-98.

Elconin, R.F. and E.R. LaChapelle. 1997. Flow and internal structure of a rock glacier. J, Glaciol., 43 (144), 238-244.

Haeberli, W. 1985. Creep of mountain permafrost: internal structure and flow of Alpine rock glaciers. Mitteilungen der Versuchsanstalt für Wasserbau, Hydrologie und Glaziologie an der Eidgenössischen Technischen Hochschule (Zürich), Nr. 77.

Haeberli W., M. Hoelzle, A. Kääb, F. Keller, D. VonderMühll and S. Wagner. 1998. Ten years after drilling through the permafrost of the active rock glacier Murtél, eastern Swiss Alps: Answered questions and new perspectives. In Proceedings 7th International Conference on Permafrost, Yellowknife, Canada. 403-409.

Harris, S.A. and D.E. Pedersen. 1998. Thermal regimes beneath coarse blocky materials. Permafrost Periglac. Process. 9, 107-120.

Hoelzle, M., S. Wagner, A. Kääb and D. Vonder Mühll. 1998. Surface movement and internal deformation of ice-rock mixtures within rock glaciers in the Upper Engadin, Switzerland. In Proceedings 7th International Conference on Permafrost, Yellowknife, Canada. 465-471.

Hooke, R. LeB., B.B. Dahlin and M.T. Kauper. 1972. Creep of ice containing dispersed fine sand. J. Glaciol., 11 (63), 327-336.

Hooke, R. LeB. 1981. Flow law for polycrystalline ice in glaciers: comparison of theoretical predictions, laboratory data, and field measurements. Rev. Geophys. Space Phys., 19(4), 664-672.

Hughes, T. 1986. The Jakobshavns Effect. Geophysical Research Letters, 13 (1), 46-48

Kääb, A., H. Gudmundsson and M. Hoelzle. 1998. Surface deformation of creeping mountain permafrost. Photogrammetric investigations on Murtél Rock Glacier, Swiss Alps. In Proceedings 7th International Conference on Permafrost, Yellowknife, Canada. 403-409.

Kamb, B. and K.A. Echelmeyer. 1986. Stress-gradient coupling in glacier flow: I. Longitudinal averaging of the influence of ice thickness and surface slope. J. Glaciol., 32 (111), 267-284.

Kaufmann, V. 1998. Deformation analysis of the Doesen Rock Glacier (Austria). In Proceedings 7th International Conference on Permafrost, Yellowknife, Canada. 403-409.

Konrad, S.K., N.F. Humphrey, E.J. Steig, D.H. Clark, N.Jr. Potter and W.T. Pfteffer. 1999. Rock glacier dynamics and paleoclimatic implications. Geology, 27 (12), 1131-1134.

Konrad, S.K. and N.F. Humphrey. 2000. Steady-state flow model of debris-covered glaciers (rock glaciers). Debris-Covered Glaciers, workshop proceedings Seattle, Washington, IAHS Pulb. No. 264. 255-263.

Nickling, W.G. and L. Bennett. 1984. The shear strength characteristics of frozen coarse granular debris. J. Glaciol., 30 (106), 348-357.

Nye, J.F. 1965. The flow of a glacier in a channel of rectangular, elliptic or parabolic cross-section. J. Glaciol., 5, 589-607.

O'Neel, S., K.A. Echelmeyer, and R.J. Motyka. *In press*. Short-term flow dynamics of a retreating tidewater glacier: LeConte Glacier, Alaska, U.S.A. J. Glaciol.

Paterson, W.S.B. 1994. *The Physics of Glaciers*, 3rd edition. Elsevier Science Ltd. New York.

Rabus, B.T. and K.A. Echelmeyer. 1997. The flow of a polythermal glacier: McCall Glacier, Alaska, U.S.A. J. Glaciol.,43 (145), 522-536.

Truffer, M., W.D. Harrison and K.A. Echelmeyer. 2001. Implications of till deformation on glacier dynamics. J. Glaciol., 47 (156), 123-134.

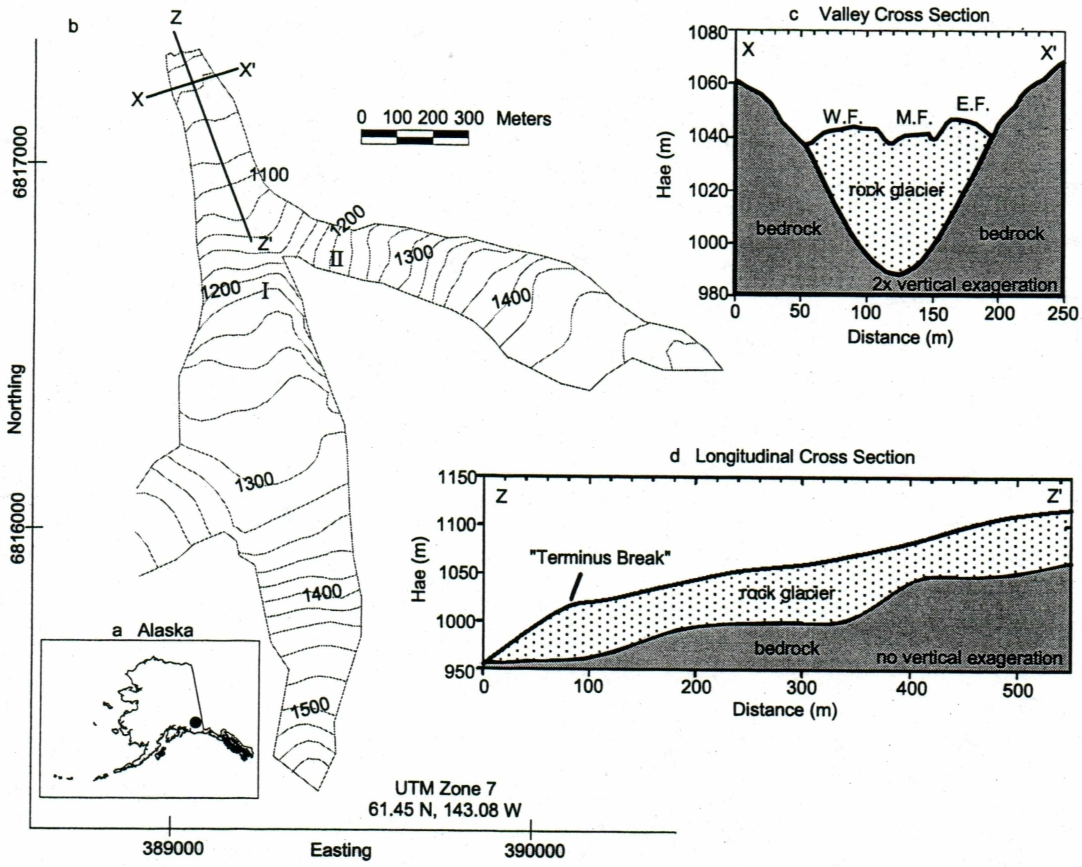

Fig. 3.1: Location, topography and geometry of Fireweed Rock Glacier. Contours are interpolated from surface profiles along the margins and centerlines of each tributary and flow. Thickness measurements in (c) and (d) are from geophysical soundings (Chapter 2). W.F., M.F., and E.F., are the West, Middle, and East Flows of the Main Trunk. I and II mark the steep sections referred to in the text.

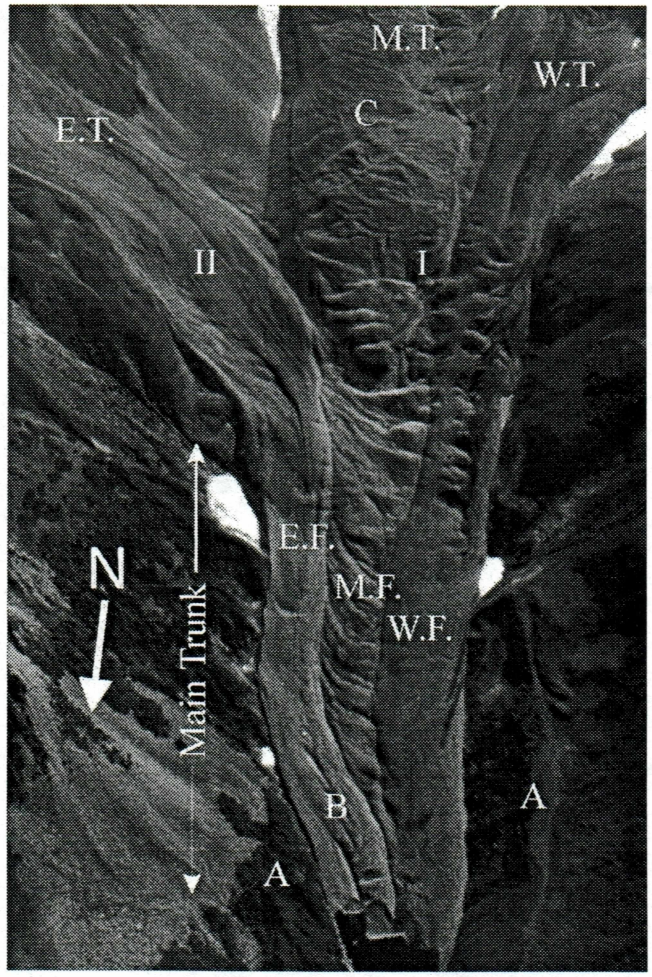

Fig. 3.2: Main Trunk overview photo. Oblique air photo showing the convergence of the three tributaries into the Main Trunk. Labels are as follow: E.T. (East Tributary), M.T. (Middle Tributary), W.T. (West Tributary), E.F., M.F., and W.F. are the respective flows. 'A' indicates lateral moraines from previous glaciation. 'B', longitudinal ridges and furrows thought to delineate the ice-rich region of E.F. I and II, the steep sections discussed in the text. (Photo by R. Elconin)

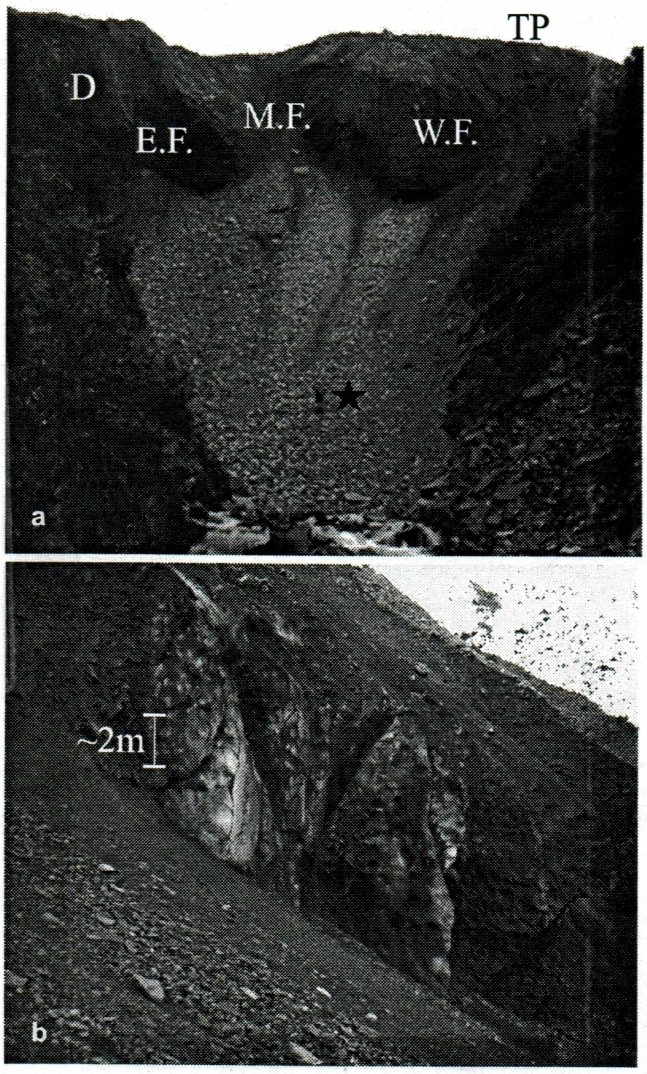

Fig. 3.3: Caved terminus photos. a) Photograph of the calved terminus in 2001. 'D' is the location of the ice-rich region. Contributions of the flows to the face are marked as E.F., M.F., and W.F. The top of the photograph is ~90 m across and note the person for scale near the bottom of the talus. (Photo by L. Cox) (b) Close-up of the ice-rich region, 2001. View is looking across the calved face from the east margin toward the west. (Photo by M. Truffer)

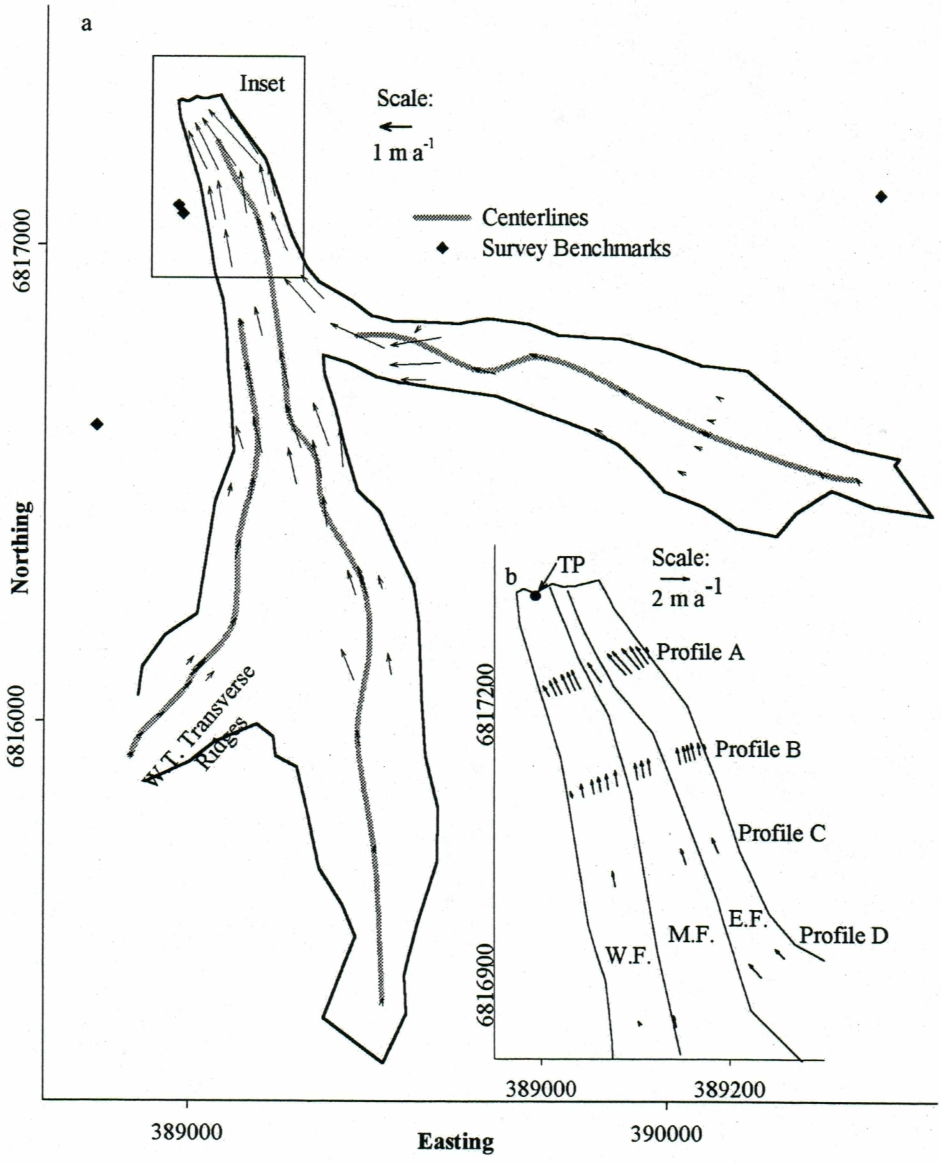

Fig. 3.4: Horizontal surface velocity coverage. Surface velocities of Fireweed Rock Glacier. Center point of the arrow marks the location of the velocity markers. (a) The entire rock glacier showing location of benchmarks denoted by diamonds. (b) Detailed diagram of the Main Trunk.

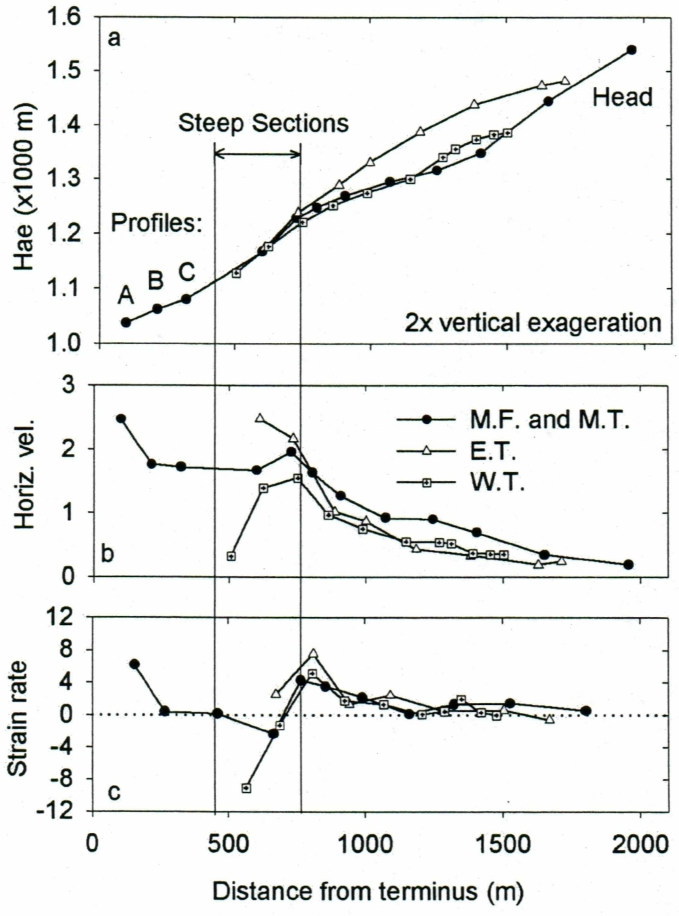

Fig. 3.5: Centerline profile, velocity and strain rate. (a) Centerline surface profile along the tributaries and Main Trunk, centerline location shown in Fig. 3.4. (b) Horizontal velocities along the profiles, and (c) strain rate between the velocity markers in (x 0.001 a^{-1}) (b).

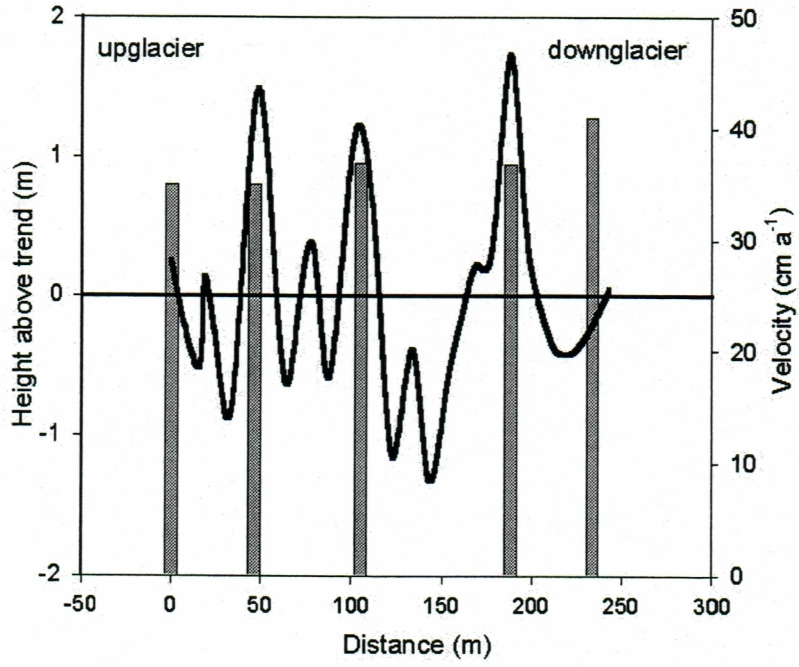

Fig. 3.6: Velocities in transverse ridges. Topography profile along transect through W.T. transverse ridges (line) and velocities along these ridges (bars). The location of this transect is shown in Fig. 3.4.

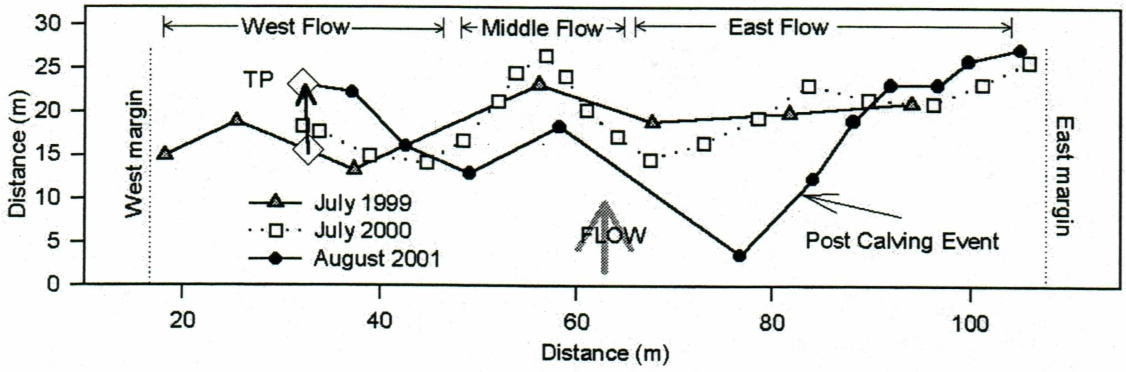

Fig. 3.7: Terminus Break position changes. Profiles along the terminus break at different times during the study. The August 2001 location shows the removal of material from the most recent calving. The velocity of TP averaged from 1999 to 2001 was 3.7 m a^{-1} (error ~0.5 m a^{-1}).

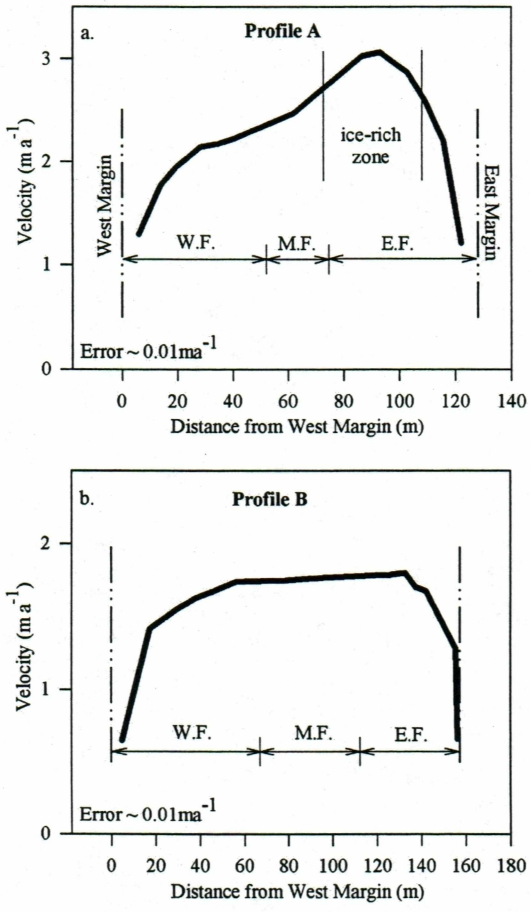

Fig. 3.8: Velocity profiles A and B. (a) Asymmetric Profile A and (b) more symmetric Profile B.

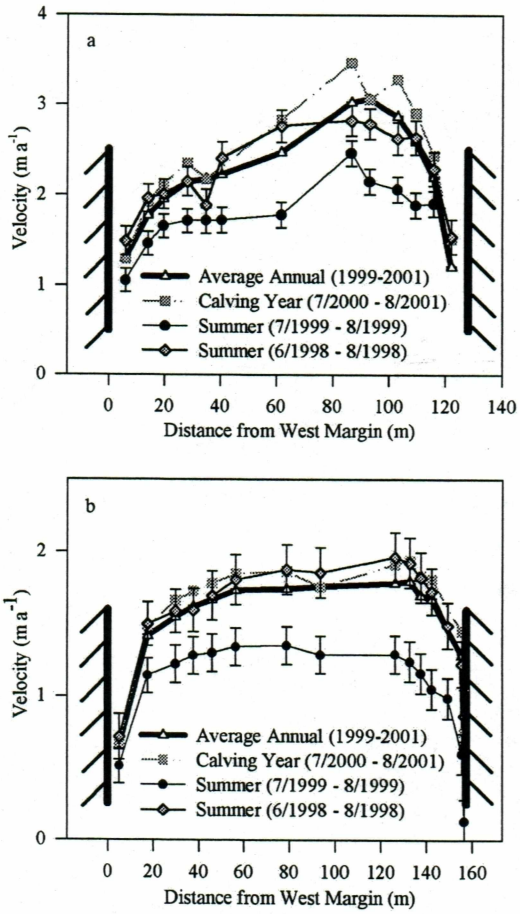

Fig. 3.9: Temporal velocity variations at profiles (a)A and (b)B.

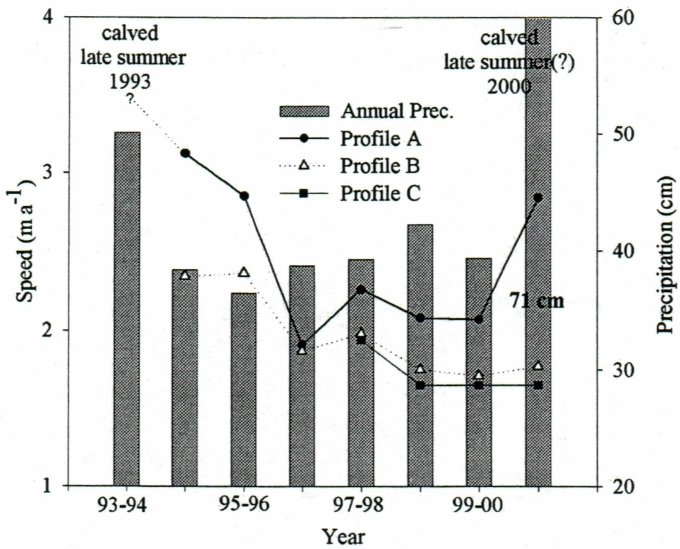

Fig. 3.10: Precipitation, velocity and calving. Annual precipitation, calving events, and annual velocities on the centerline at Profiles A,B, and C.

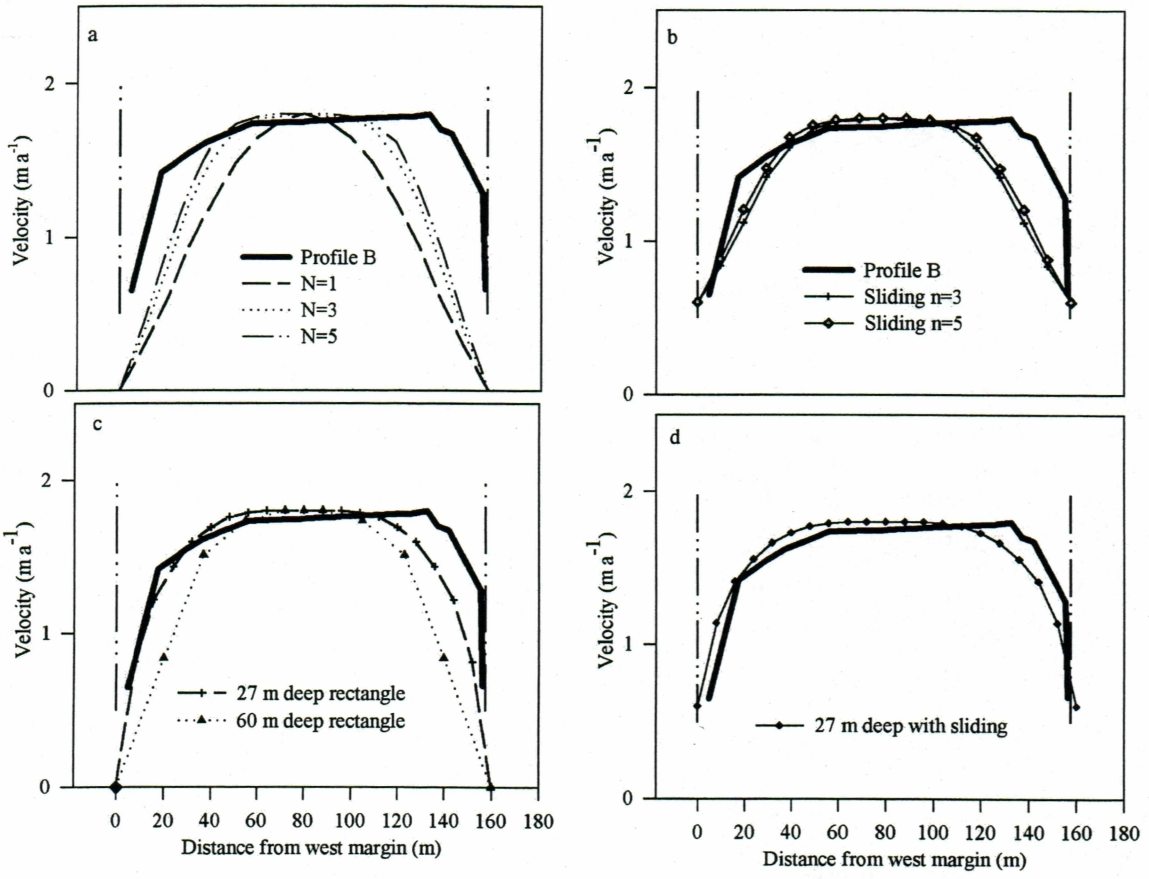

Fig. 3.11: Channel flow analysis. (a) modeled flow in a parabolic channel for various values of *n*, (b) parabolic channel solutions with sliding, (c) rectangular channel for various channel depths, (d) reasonable fit to Profile B velocities, shallow (~27 m) channel with sliding and n = 3.

CHAPTER 4:

SUMMARY

With geophysical methods we have investigated the geometry of Fireweed Rock Glacier. From this geometry and surface velocity measurements we analyzed the flow. With transient electromagnetic methods we were able to determine rock glacier thickness and with seismic surveys we were able to resolve the debris mantle thickness and identify a discontinuity within the mélange. Analysis suggests that the discontinuity is the focus of much of the motion. We infer that "sliding" occurs along a shear plane at this discontinuity (~27 m depth) and deformation occurs above this. Our best fit model, which is non-unique, indicates that the mélange is about 2 times softer than clean glacier ice. This is consistent with other observations of debris laden ice found at the base of ice glaciers. Fireweed Rock Glacier is also very fast — flowing over 3.5 m a^{-1} within the Main Trunk —on most other rock glaciers, surface velocities seldom exceed 1 m a^{-1}. The flow of this rock glacier is also interesting in that it exhibits seasonal variations in flow. We have also detected an influence on flow by the quasi-periodic calving of the terminus and rainfall events. This behavior is similar to that observed on tidewater glaciers, which also calve.

Applications of transient electromagnetic methods to glaciology are uncommon. This method is very good at determining the geometry of a rock glacier. This study also

indicates that it may be a effective means of locating the distribution of tills beneath glaciers and rock glaciers alike.

COMPREHENSIVE LITERATURE CITED

Andersland, O.B., B. Ladanyi. 1984. An introduction to frozen ground engineering. Chapman and Hall. New York.

Barsch, D. 1987. The problem of the ice-cored rock glacier. In: Giardino, J.R., Shroder, J.F.Jr., and Vitek, J.D., Eds. Rock Glaciers. Allen and Unwin. Boston. 45-53.

Cohen, D. 2000. Rheology of ice at the bed of Engabreen, Norway. J. Glaciol., 46 (155), 611-621.

Costello D.P. 2000. Seismic and geomorphic investigations of Galena Creek Rock Glacier. Master's Thesis, University of Colorado, Boulder, Colorado.

Echelmeyer, K.A. 1983. Response of Blue Glacier to a perturbation in ice thickness: theory and observation. Doctoral Thesis, California Institute of Technology, Pasadena California.

Echelmeyer, K.A. and Z. Wang. 1987. Direct observation of basal sliding and deformation of basal drift at sub-freezing temperatures. J. Glaciol., 33 (113), 83-98.

Elconin, R.F. 1985. Internal composition, structure, and genesis of an active and well developed compound rock glacier, Wrangell Mountains, Alaska. Master's Thesis, Humboldt State University, Arcata, California.

Elconin, R.F. and E.R. LaChapelle. 1997. Flow and internal structure of a rock glacier. J, Glaciol., 43 (144), 238-244.

Evin, M., D. Fabre and P.G. Johnson. 1997. Electrical resistivity measurements on the rock glaciers of Grizzly Creek, St. Elias Mountains, Yukon. Permafrost Periglac. Process. 8. 179-189.

Fisch, W.Sr., W.Jr. Fisch and W. Haberli. 1977. Electrical resistivity soundings with long profiles on rock glaciers and moraines in the Alps of Switzerland. Zeitschrift für Gletscherkunde und Glazialgeologie, 13 (1/2), 239-260.

Haeberli, W. 1985. Creep of mountain permafrost: internal structure and flow of Alpine rock glaciers. Mitteilungen der Versuchsanstalt für Wasserbau, Hydrologie und Glaziologie an der Eidgenössischen Technischen Hochschule (Zürich), Nr. 77.

Haeberli W., M. Hoelzle, A. Kääb, F. Keller, D. VonderMühll and S. Wagner. 1998. Ten years after drilling through the permafrost of the active rock glacier Murtél, eastern Swiss Alps: Answered questions and new perspectives. In Proceedings 7th International Conference on Permafrost, Yellowknife, Canada. 403-409.

Harris, S.A. and D.E. Pedersen. 1998. Thermal regimes beneath coarse blocky materials. Permafrost Periglac. Process. 9, 107-120.

Hauck, C., M. Guglielmin, K. Isaksen and D. Vonder Muhll. 2001. Applicability of frequency-domain and time-domain electromagnetic methods for mountain permafrost studies. Permafrost Periglac. Process. 12 (1), 39-52.

Hoelzle, M., S. Wagner, A. Kääb and D. Vonder Mühll. 1998. Surface movement and internal deformation of ice-rock mixtures within rock glaciers in the Upper Engadin, Switzerland. In Proceedings 7th International Conference on Permafrost, Yellowknife, Canada. 465-471.

Hooke, R. LeB., B.B. Dahlin and M.T. Kauper. 1972. Creep of ice containing dispersed fine sand. J. Glaciol., 11 (63), 327-336.

Hooke, R. LeB. 1981. Flow law for polycrystalline ice in glaciers: comparison of theoretical predictions, laboratory data, and field measurements. Rev. Geophys. Space Phys., 19(4), 664-672.

Hughes, T. 1986. The Jakobshavns Effect. Geophysical Research Letters, 13 (1), 46-48

Kääb, A., H. Gudmundsson and M. Hoelzle. 1998. Surface deformation of creeping mountain permafrost. Photogrammetric investigations on Murtél Rock Glacier, Swiss Alps. In Proceedings 7th International Conference on Permafrost, Yellowknife, Canada. 403-409.

Kamb, B. and K.A. Echelmeyer. 1986. Stress-gradient coupling in glacier flow: I. Longitudinal averaging of the influence of ice thickness and surface slope. J. Glaciol., 32 (111), 267-284.

Kaufman, A. A. 1979. Harmonic and transient fields on the surface of a two-layer medium: Geophysics, 44, 1208-1217.

Kaufman, A.A. and G.V. Keller. 1983. Frequency and transient Soundings. Elsevier. New York. 695 p.

Kaufmann, V. 1998. Deformation analysis of the Doesen Rock Glacier (Austria). In Proceedings 7th International Conference on Permafrost, Yellowknife, Canada. 403-409.

Keller, G.V. 1991. Rock and mineral properties: in Nabighian, M.N., Ed., Electromagnetic methods in applied geophysics, Vol 2, Soc. Expl. Geophys., 13-51.

Konrad, S.K., N.F. Humphrey, E.J. Steig, D.H. Clark, N.Jr. Potter and W.T. Pfteffer. 1999. Rock glacier dynamics and paleoclimatic implications. Geology, 27 (12), 1131-1134.

Konrad, S.K. and N.F. Humphrey. 2000. Steady-state flow model of debris-covered glaciers (rock glaciers). Debris-Covered Glaciers, workshop proceedings Seattle, Washington, IAHS Pulb. No. 264. 255-263.

MacKevett, E.M. and J.G. Smith. 1972. Geologic Map of the McCarthy B-6 Quadrangle, Alaska: U.S. Geological Survey, 1 sheet.

Nabighian, M.N. and J.C. Macnae. 1991. Time domain electromagnetic prospecting methods: in Nabighian, M.N., Ed., Electromagnetic methods in applied geophysics, Vol 2, Soc. Expl. Geophys., 427-478.

Nabighian, M.N. 1979. Quasi-static transient response of a conducting half-space — An approximate representation. Geophysics, 44, 1700-1705.

Nickling, W.G. and L. Bennett. 1984. The shear strength characteristics of frozen coarse granular debris. J. Glaciol., 30 (106), 348-357.

Nye, J.F. 1965. The flow of a glacier in a channel of rectangular, elliptic or parabolic cross-section. J. Glaciol., 5, 589-607.

O'Neel, S., K.A. Echelmeyer, and R.J. Motyka. *In press*. Short-term flow dynamics of a retreating tidewater glacier: LeConte Glacier, Alaska, U.S.A. J. Glaciol.

Paterson, W.S.B. 1994. The Physics of Glaciers, 3rd edition. Elsevier Science Ltd. New York.

Petrenko, V.F. and R.W. Whitworth. 1999. Physics of ice. Oxford University Press. New York. 373 p.

Rabus, B.T. and K.A. Echelmeyer. 1997. The flow of a polythermal glacier: McCall Glacier, Alaska, U.S.A. J. Glaciol.,43 (145), 522-536.

Truffer, M., W.D. Harrison and K.A. Echelmeyer. 2001. Implications of till deformation on glacier dynamics. J. Glaciol., 47 (156), 123-134.

Vonder Muhll, D., C. Hauck, H. Gubler, R. McDonald and N. Russill. 2001. New geophysical methods of investigating the nature and distribution of mountain permafrost with special reference to radiometry techniques. Permafrost Periglac. Process. 12 (1), 27-38.

Zonge, K.L. 1992. Chapter 6, Electromagnetics, broad band electromagnetic systems: in Van Blaricom, R., Ed., Practical geophysics II for the exploration geologist. Northwest Mining Association. Spokane, WA. 439-535.

APPENDICIES

APPENDIX 1: TRANSVERSE TEM PROFILE

In addition to the longitudinal TEM profile in Figure 2.7, a transverse profile was also made about 150 m upglacier from the terminus. This profile began on the talus slope that flanks (but does not feed) the Main Trunk on the west side. Soundings were made at about 10 m intervals using a 20 m transmitter loop. The transect crossed the rock glacier perpendicular to flow and extended up past the glacial moraine (Fig. 2.1) on the east side and ended at the position "**B**" in Figure 2.1. The center position of each of these soundings was measured with optically surveyed from BM1 (Appendix 3.1).

This transverse profile indicates a conductive feature centered beneath the western portion of the Main Trunk (Fig. 2.8). This same conductive body, interpreted to be a subglacial till or water saturated bedrock, is likely that which is apparent in the longitudinal profile shown in Figure 2.7. These two profiles are consistent with a ribbon-like distribution of till beneath the rock glacier. Although Figure 2.8 does not strongly show an interface between the mélange and the bedrock, it does identify the location of a possible conductive layer. One implication is that maybe with TEM it may be possible to map till distribution beneath glaciers and rock glaciers, even when narrow channel geometry may be present. The location of the underlying layer shown in Figure 2.8 suggests that a basal till or other conductive layer is distributed in an asymmetric way along the bed. This is consistent with the asymmetry in channel shape observed at the terminus, as is shown in the inset in this figure.

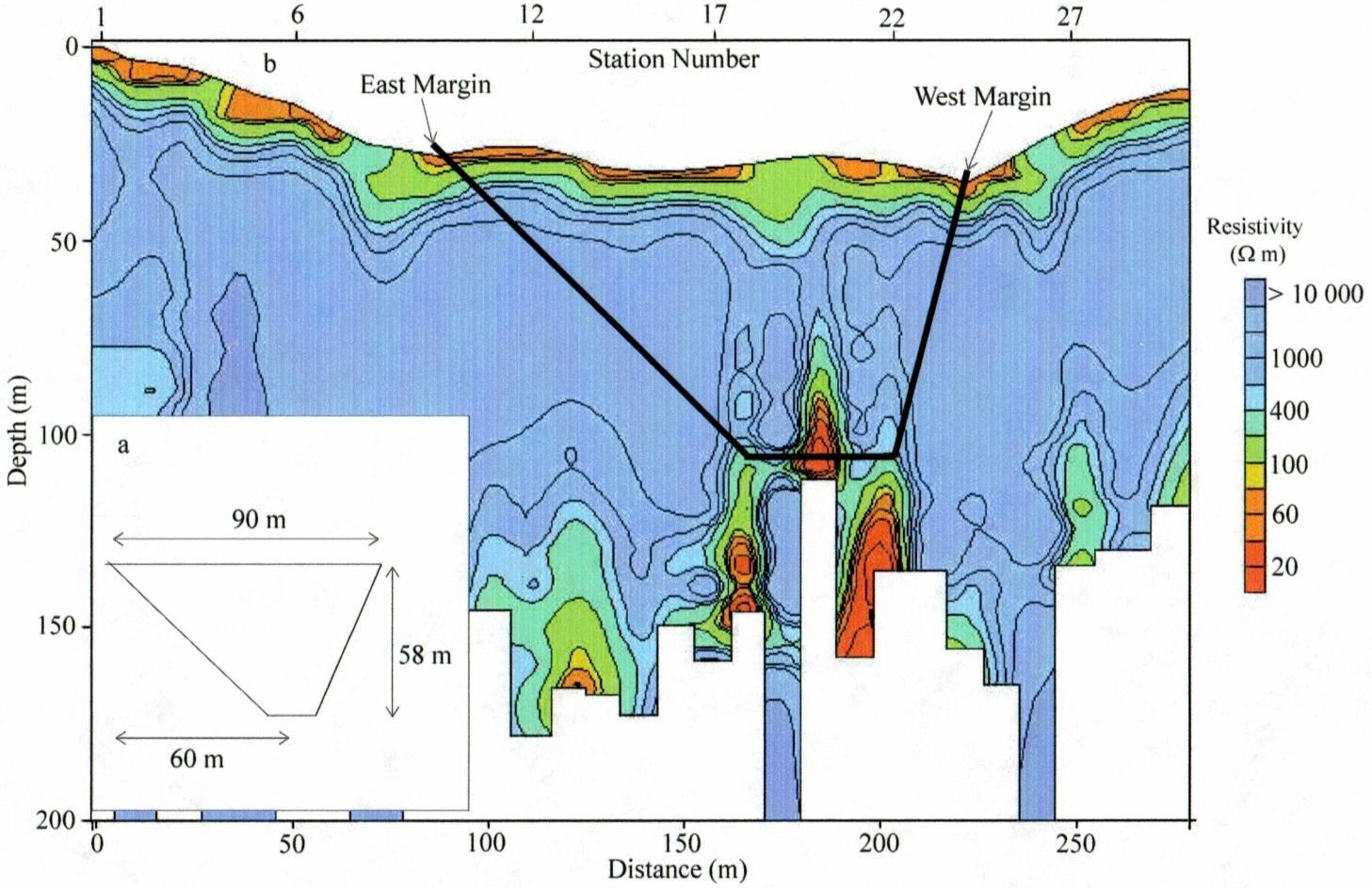

Fig. A-1: TEM transverse pseudo-section. (a) Asymmetric trapezoid geometry measured at the terminus. (b) Pseudo-section showing location of conductive till with overlain asymmetrical geometry (thick black line) consistent with terminus channel geometry and a ribbon of till situated at the bottom of the channel.

APPENDIX 2: LOCATION OF BENCHMARKS AND VELOCITY MARKERS

Surveying of the velocity markers and the topography was done from a network of 4 benchmarks. These benchmarks were constructed and surveyed relative to each other in 1997. They defined a local coordinate system that in July, 1999 was tied to the WGS 84 reference system with GPS using the National Geodetic Survey marker designated McCarthy PID: UV4128 (This marker and Fireweed Rock Glacier are found within the McCarthy B-5 Quadrangle, Alaska; UTM Zone 7). The four benchmarks are designated BM1-BM5. BM1 and BM4 were tied to the geodetic reference and the others were surveyed in reference to these. The local coordinate system was defined by BM1 and BM4 as the approximate East-West axis. Perpendicular to this, was defined an approximate North-South axis. This coordinate system was -2.1467° from UTM-north (West from North). All stake positions were first measured in the local coordinate system and then later converted to UTM position by a simple rotation about BM1. Calculations were carried out within the local coordinate system. Table 3.2 gives the local coordinates and UTM coordinates for the benchmarks.

BM	X	Y	Z	Easting	Northing	Height
1	2000	2000	3500	388984.572	6817064.665	1065.355
2	1991.234	2017.976				
4	3060.564	2000	3897.123	6817104.361	390043.557	14650.097
5	1805.843	1562.662	3778.124			

Table A-1: Survey benchmark data. Local coordinates given in X (~north),Y(~east) and Z(vertical). UTM in Easting, Northing and Height (msl). Height is in msl at it may be converted to height above ellipsoid (Hae) by adding 18.18 m.

Velocity markers on the Main Trunk and both steep sections (I and II; Fig. 3.1) were surveyed from BM1 with horizontal reference set at BM2. The entire West Tributary and the remainder of the Middle Tributary above the steep section were surveyed from BM5 with horizontal reference set at BM1. The East Tributary above the steep section was surveyed from BM4 with horizontal reference again set to BM1. The local coordinate position and average horizontal velocity from July 1999 to August 2001 of each marker is given in Table A-2.

Table A-2: Velocity markers: positions and velocities.

Stake	Hz Vel	HzVelErr	Easting	Northing	Hae
lr1	1.21	0.01	389113.735	6817235.148	1046.892
lr2	2.2	0.01	389107.833	6817232.848	1046.534
lr3	2.59	0.01	389101.804	6817230.655	1047.033
lr4	2.87	0.01	389095.745	6817228.379	1046.646
lr5a	2.42	0.01	389099.545	6817210.049	1048.826
lr5	3.06	0.01	389086.47	6817224.809	1045.118
lr5b	3.81	0.01	389073.057	6817238.44	1041.186
lr6	3.02	0.01	389080.354	6817222.568	1043.581
ur1	0.66	0.01	389173.572	6817133.73	1060.721
ur2	1.28	0.01	389167.688	6817131.59	1061.41
ur3a	1.75	0.01	389167.925	6817111.093	1067.772
ur3	1.76	0.02	389161.094	6817129.199	1062.389
ur3b	1.73	0.02	389153.992	6817147.454	1059.546
ur4	1.67	0.01	389156.656	6817127.548	1062.355
ur5	1.7	0.01	389152.26	6817125.933	1062.354
ur6	1.8	0.01	389146.111	6817123.722	1062.344
rf1	1.72	0.01	389184.511	6817027.863	1082.263
rf2	1.38	0.01	389253.7	6816912.735	1125.141
rf3	1.94	0.01	389227.555	6816894.499	1122.793
rf4	2.48	0.01	389349.122	6816810.599	1174.107
rf5	0.38	0.02	389475.782	6816824.184	1237.332
rf6	2.17	0.02	389472.258	6816799.182	1237.349
rf7	2.12	0.02	389470.779	6816751.907	1231.836

Table A-2: Continued

Stake	Hz Vel	HzVelErr	Easting	Northing	Hae
rf8	1.05	0.02	389467.363	6816718.079	1235.298
rf9	1.02	0.02	389615.9	6816736.617	1288.773
rf10	0.87	0.02	389732.154	6816766.66	1330.777
rf11	0.43	0.02	389909.52	6816693.519	1386.507
rf12	0.58	0.02	389861.48	6816607.072	1391.782
rf13	0.17	0.02	390105.828	6816681.514	1435.151
rf14	0.26	0.02	390090.414	6816631.954	1436.101
rf15a	9.55	0.02	390091.133	6816602.422	1438.825
rf15	0.33	0.02	390081.784	6816605.015	1437.561
rf15b	0.27	0.04	390072.441	6816607.591	1435.858
rf16	0.35	0.02	390064.137	6816575.382	1433.008
rf17	0.4	0.02	390030.407	6816521.762	1435.124
rf18	0.19	0.02	390319.195	6816521.308	1472.67
rf19	0.24	0.02	390395.607	6816507.658	1481.026
lm1	2.47	0.01	389057.232	6817213.795	1037.256
um1	1.78	0.01	389115.386	6817112.51	1060.049
um2a	1.78	0.01	389114.259	6817091.439	1063.914
um2	1.76	0.01	389108.369	6817109.896	1061.825
um2b	1.69	0.02	389102.293	6817128.593	1057.57
um3	1.75	0.01	389101.651	6817107.371	1063.119
mf1	1.72	0.01	389151.53	6817016.067	1079.675
mf2	1.26	0.01	389142.138	6816840.319	1126.795
mf3	1.67	0.02	389197.114	6816737.985	1166.162
mf4	1.92	0.02	389274.346	6816623.127	1233.492
mf5	1.96	0.02	389216.42	6816618.995	1227.157
mf6	1.66	0.02	389317.158	6816574.852	1243.302
mf7	1.64	0.02	389266.652	6816549.314	1246.476
mf8	1.55	0.02	389214.007	6816534.73	1240.404
mf9	1.27	0.02	389283.766	6816438.782	1268.34
mf10	0.56	0.02	389399.852	6816292.265	1295.919
mf11a	0.89	0.02	389365.045	6816284.018	1295.501
mf11	0.92	0.02	389362.399	6816293.653	1294.291
mf11b	0.94	0.02	389360.073	6816303.076	1292.958
mf12	1.05	0.02	389339.108	6816291.837	1291.693
mf13	0.9	0.03	389418.993	6816121.553	1315.348
mf14	1.42	0.03	389330.895	6816119.507	1306.436
uf1	0.69	0.03	389353.602	6815964.895	1347.607

Table A-2: Continued

uf2	0.34	0.03	389388.245	6815729.376	1443.565
uf3	0.19	0.04	389404.931	6815412.912	1539.865
ll1	2.22	0.01	389037.21	6817206.192	1039.368
ll2	2.17	0.01	389031.922	6817204.119	1040.307
ll3	2.14	0.01	389025.721	6817201.761	1040.712
ll4	1.95	0.01	389017.774	6817198.758	1040.586
ll4a	1.9	0.01	389025.335	6817180.677	1046.268
ll4b	2.08	0.01	389010.208	6817216.749	1035.107
ll5	1.77	0.01	389012.576	6817196.836	1039.873
lf1	1.59	0.01	389077.983	6816991.921	1083.423
lf2	0.32	0.01	389104.602	6816839.091	1128.408
lf3	1.39	0.01	389124.004	6816718.516	1176.137
lf4	1.55	0.02	389141.95	6816599.446	1220.61
lf5	0.97	0.02	389103.407	6816594.501	1217.854
lf6	0.97	0.02	389129.778	6816485.662	1250.537
lf7	0.55	0.02	389083.797	6816484.574	1252.67
lf8	0.75	0.02	389101.539	6816360.291	1273.673
lf9	0.55	0.02	389092.491	6816206.64	1299.528
lf10	0.53	0.02	389044.246	6816094.975	1340.297
lf11a	0.53	0.02	389014.93	6816106.061	1343.322
lf11	0.54	0.02	389020.933	6816113.945	1340.13
lf11b	0.54	0.02	389026.691	6816121.258	1336.987
lf12	0.49	0.02	389003.309	6816127.607	1338.512
lf13	0.52	0.02	388997.522	6816074.853	1355.866
lf14	0.37	0.02	388941.089	6816013.192	1373.487
lf15	0.35	0.02	388899.096	6815970.171	1381.852
lf16	0.35	0.02	388880.105	6815927.8	1385.693

Table A-2: Velocity markers: positions and velocities. Two year average horizontal velocity of each marker and the error. Position of each marker is given in UTM coordinates for UTM Zone 7. Hae is height above ellipsoid (Geoid 96).

APPENDIX 3: EMERGENCE VELOCITIES

Emergence velocity is the rate of vertical rise or subsidence of the rock glacier's surface:

$$v_E = v + u_H \tan \alpha_l \qquad \text{(A-1)}$$

where v and u_H are the vertical (positive upward) and horizontal components of surface velocity and α_l is the local surface slope, positive downward. On an ice glacier, v_E is generally negative in the accumulation area and positive in the ablation area. In steady state, v_E is equal and opposite to the annual mass balance rate, $\dot{b}$. If the glacier is not in steady state then the rate of change in the thickness at a fixed position is

$$\dot{h} = v_E + \dot{b} \qquad \text{(A-2)}$$

We calculated the emergence velocities on the rock glacier using the two-year average velocity components. Using estimated errors of 0.05 and 0.02 in v and u_H, respectively. We estimate an uncertainty in v_E of up to 0.1 m a^{-1}, being dominated by errors in slope and the averaging length for slope. The pattern of emergence velocities at Fireweed Rock Glacier (Fig. A-2) does not follow that expected for a simple ice glacier, as there is no distinct position where v_E switches from negative to positive values, as at the equilibrium-line of an ice glacier. The emergence velocities are all very near zero except within the steep section. The large calculated emergence velocities there are probably due to large errors in surface slope. The near-zero emergence velocities everywhere else indicate a very different flow pattern than on ice glaciers.

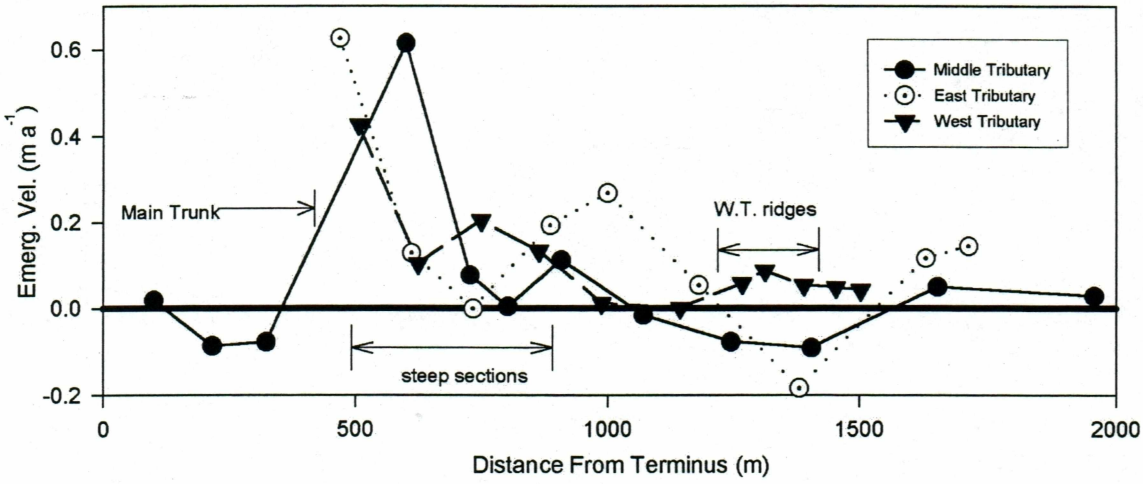

Fig. A-2: Emergence velocities along centerline of tributaries. Centerlines of each flow along which these velocities were calculated are shown in Fig. 3.4.